JPET Fast Forward. Published on June 7, 2019 as DOI: 10.1124/jpet.119.259499
This article has not been copyedited and formatted. The final version may differ from this version.

JPET # 259499

Heteromeric neuronal nicotinic acetylcholine receptors with mutant beta subunits acquire sensitivity to α7-selective positive allosteric modulators

Clare Stokes, Sumanta Garai, Abhijit R. Kulkarni, Lucas N. Cantwell, Colleen M. Noviello, Ryan E. Hibbs, Nicole A. Horenstein, Khalil A. Abboud, Ganesh A. Thakur, and Roger L. Papke

Department of Pharmacology and Therapeutics, University of Florida, PO Box 100267, Gainesville FL, 32610-0267 (CS, RLP)

Department of Pharmaceutical Sciences, School of Pharmacy, Bouvé College of Health Sciences, Northeastern University, Boston, MA 02115 (SG, ARK, LNC, GAT)

Department of Chemistry, University of Florida, Gainesville, FL 32611-7200 (NAH, KAA)

Department of Neuroscience, UT Southwestern Medical Center, Dallas TX 75390-9111 (CMN, REH)

JPET # 259499

Running title: Mutant heteromeric nAChR sensitive to α7 PAMs

*To whom correspondence should be addressed:

Name: Roger L. Papke

Phone: 352-392-4712

Fax: 352-392-3558

E-mail: rlpapke@ufl.edu

Address: Department of Pharmacology and Therapeutics

University of Florida

P.O. Box 100267

Gainesville, FL 32610-0267

Number of text pages:.....29

Number of tables:.....1

Number of figures:.....13

Number of references:.....73

Number of words in Abstract:.....250

Number of words in Introduction: 705

Number of words in Discussion:.....1474

Abbreviations: A-867744, 4-(5-(4-chlorophenyl)-2-methyl-3-propionyl-1H-pyrrol-1-yl)benzenesulfonamide: ACh, acetylcholine; ago-PAM, allosteric activating positive allosteric modulator; CAP, cholinergic anti-inflammatory pathway; DAA, direct allosteric activation; GAT107, ((3aR,4S,9bS)-4-(4-bromophenyl)-3a,4,5,9b-tetrahydro-3H-cyclopenta[c]quinoline-8-sulfonamide); nAChR, nicotinic acetylcholine receptor; PAMs, Positive allosteric modulators; PNU-120596 (1-(5-chloro-2,4-dimethoxyphenyl)-3-(5-methylisoxazol-3-yl)-urea); GAT927, 4-(4,5,6,7-tetrahydrobenzo[b]thiophen-3-yl)-3a,4,5,9b-tetrahydro-3H-cyclopenta[c]quinoline-8-sulfonamide; TM1, first transmembrane domain; TM2, second transmembrane domain; TQS, 3a,4,5,9b-Tetrahydro-4-(1-naphthalenyl)-3H-cyclopentan[c]quinoline-8-sulfonamide; α-BTX, α-bungarotoxin

Recommended section assignment: Neuropharmacology

Abstract

Homomeric α7 nicotinic acetylcholine receptors (nAChR) have an intrinsically low probability of opening that can be overcome by α7-selective positive allosteric modulators (PAMs), which bind at a site involving the second transmembrane domain (TM2). Mutation of a methionine that is unique to α7 at the 15' position of TM2 to leucine, the residue in most other nAChR subunits, largely eliminates the activity of such PAMs. We tested the effect of the reverse mutation (L15'M) in heteromeric nAChR receptors containing α4 and β2, the nAChR subunits that are most abundant in brain. Receptors containing these mutations were found to be strongly potentiated by the α7 PAM TQS but insensitive to the alternative PAM PNU-120596. The presence of the mutation in the β2 subunit was necessary and sufficient for TQS sensitivity. The primary effect of the mutation in the α4 subunit was to reduce responses to ACh applied alone. Sensitivity to TQS required only a single mutant β subunit, regardless of the position of the mutant β subunit within the pentameric complex. Similar results were obtained when β2L15'M was co-expressed with α2 or α3 and when the L15'M mutation was placed in β4 and co-expressed with α2, α3, or α4. Functional receptors were not observed when β1L15'M subunits were co-expressed with other muscle nAChR subunits. The unique structure-activity relationship of PAMs and the α4β2L15'M receptor compared to α7, and the availability of high resolution α4β2 structures may provide new insights into the fundamental mechanisms of nAChR allosteric potentiation.

Significance Statement

Heteromeric neuronal nAChRs, have a relatively high initial probability of channel activation compared to receptors that are homomers of α7 subunits but are insensitive to positive allosteric modulators (PAMs), which greatly increase the open probability of α7 receptors. These features of heteromeric nAChR can be reversed by mutation of a single residue present in all neuronal heteromeric nAChR subunits to the sequence found in α7. Specifically, the mutation of the TM2 15' leucine to methionine in alpha subunits reduces heteromeric receptor channel activation, while the same mutation in neuronal β subunits allows heteromeric receptors to respond to select α7 PAMs. The results indicate a key role for this residue in the functional differences in the two main classes of neuronal nAChR.

Introduction

The two main nicotinic acetylcholine receptors (nAChR) in brain can be identified by their high affinity binding either to acetylcholine (ACh) and nicotine or to α-bungarotoxin (Clarke et al., 1985). Receptors with high affinity for ACh and nicotine are heteromeric pentamers combining α and non-α (β) subunits, the most widely-expressed subunits being α4 and β2 (Wada et al., 1989). The receptors binding α-bungarotoxin are strongly expressed in the hippocampus and other brain areas related to cognition and function as homomeric pentamers containing the α7 subunit (Wada et al., 1989). The expression pattern of α7 nAChR suggested that they might be a target for the treatment of Alzheimer's disease and other cognitive disorders (Levin and Rezvani, 2000; Mazurov et al., 2006). α7 nAChR also play an essential role in non-neuronal cells as mediators of a cholinergic anti-inflammatory pathway (CAP) (Wang et al., 2003; Rosas-Ballina and Tracey, 2009).

As noted above, α7 nAChR have low affinity for ACh. However, in heterologous expression systems they most effectively activate in the same micromole ACh concentration range that best activates heteromeric receptors like those containing α4 and β2 subunits (Papke and Thinschmidt, 1998; Papke and Papke, 2002). The key difference between these two main neuronal nAChR subtypes relates to their desensitization processes. After a brief period of high probability channel opening, heteromeric receptors convert to desensitized states that bind ACh and nicotine with high affinity (Campling et al., 2013). Under normal conditions, α7 receptors never open with high probability and rapidly enter non-conducting desensitized states that are associated with high levels of agonist binding and are unique to α7 (Uteshev et al., 2002; Williams et al., 2012).

Our understanding of the unique activation and desensitization properties of α7 nAChR has been advanced by the discovery of numerous positive-allosteric modulators

(PAMs) that selectively affect α7 receptors (Williams et al., 2011b). The most efficacious of these agents, identified as type II PAMs (Gronlien et al., 2007), appear to promote a unique conformational state associated with the destabilization of non-conducting "desensitized" states, resulting in protracted bursts of channel opening (Williams et al., 2011a; Andersen et al., 2016). The potential therapeutic utility of such PAMs for both CNS (Williams et al., 2011b) and peripheral indications such as inflammatory pain (Freitas et al., 2013; Bagdas et al., 2016) is an active area of research.

Investigations of the structural basis for α7-PAM activity has been impeded by the lack of high-resolution crystal structures or homology models of α7 that include the pore-forming transmembrane domains. Nonetheless, studies of receptor chimeras and mutants, using the 5HT3A receptor sequence as a negative control, have generated good evidence for a PAM binding site associated with the first and second transmembrane domains (TM1 and TM2, respectively) (Young et al., 2008). The sequence of the pore-forming TM2 (Akabas et al., 1994) is highly conserved among the nAChR subunits (Figure 1).

Starting with α7/5HT3A chimeras, two point mutations were identified that had equivalently large effects on reducing PNU-120596 potentiation (Young et al., 2008). One mutant, α7A226D, substituted a residue that is unique to 5HT3A (Figure 1) for a residue that is present in α7, but also in several other nAChR subunits. The single most important residue for the α7-selective PAM activity of PNU-129596, which is unique to the α7 sequence, was the methionine residue at the 15' position (residue 254 in the human α7). Since the conversion of this residue to a leucine, which is the corresponding residue in most other nAChR subunits (all but α9 and α10), causes the essential loss of α7 PAM activity (Young et al., 2008; Quadri et al., 2019), we tested the effects of the reverse mutation (L15'M) on the sensitivity of heteromeric nAChR to PAMs that are normally only effective on α7 receptors.

We report that this single point mutation in neuronal beta subunits is sufficient to generate heteromeric nAChR that are sensitive to potentiation by select α7 PAMs. Furthermore, this site in α4β2 nAChR differentiates among structural classes of PAMs differently than it does in α7 receptors. The structure-activity profile of PAMs active on α4β2 mutants and the availability of crystallographic and cryo-electron microscopy structures of α4β2 (Morales-Perez et al., 2016; Walsh et al., 2018) may provide new insights into the nature of this allosteric modulation.

JPET Fast Forward. Published on June 7, 2019 as DOI: 10.1124/jpet.119.259499
This article has not been copyedited and formatted. The final version may differ from this version.

Materials and methods

Commercial reagents

Acetylcholine chloride (ACh), atropine, and other chemicals were purchased from Sigma-Aldrich Chemical Company (St. Louis, MO). GAT107 ((3aR,4S,9bS)-4-(4-bromophenyl)-3a,4,5, 9b-tetrahydro-3H-cyclopenta[c]quinoline-8-sulfonamide) (Kulkarni and Thakur, 2013; Thakur et al., 2013) and B-973B (3-(3,4-difluorophenyl)-N-(1-(6-(4-(pyridin-2-yl)piperazin-1-yl)pyrazin-2-yl)ethyl)propenamide) (Garai et al., 2018), and PNU-120596 (Williams et al., 2011a) were synthesized as described previously. Fresh ACh stock solutions were made in Ringer's solution each day of experimentation. Stock solutions of the PAMs were made in DMSO and kept at -20ºC and diluted in Ringer's solution each day.

Compound Synthesis

4-(4,5,6,7-tetrahydrobenzo[b]thiophen-3-yl)-3a,4,5,9b-tetrahydro-3H-cyclopenta[c]quinoline-8-sulfonamide (GAT927):

4,5,6,7-tetrahydrobenzo[b]thiophene-3-carbaldehyde (100 mg, 0.6 mM), sulfanilamide (103 mg, 0.6 mM) and indium chloride (40 mg, 0.18 mM) were dissolved in anhydrous acetonitrile in a 10 ml microwave vial. Freshly distilled cyclopentadiene (119 mg, 1.8 mM) was added to the reaction mixture and irradiated under microwave for 15 min at 60˚C. The reaction mixture was quenched with saturated aqueous solution Na2CO3. The aqueous layer was extracted with ethyl acetate (3×5 ml) and combined organic layer was dried over anhydrous Na_2SO_4 followed by evaporated under reduced pressure. The crude reaction mixture was purified by silica gel column chromatography to yield pure GAT927 (224 mg, 98%) as off white solid.

1H NMR (CDCl3, 500 MHz): δ 7.59 (s, 1H), 7.51 (dd, J=8.6, 2.0 Hz, 1H), 7.03 (s, 1H), 6.63 (d, J=8.4 Hz, 1H), 5.85-5.84 (m, 1H), 5.70-5.69 (m, 1H), 4.64-4.62 (m, 3H), 4.16 (s, 1H), 4.07 (d, J=9.7 Hz, 1H), 3.08-3.02 (m, 1H), 2.82-2.79 (m, 2H), 2.61-2.51 (m, 3H), 1.97-1.92 (m, 1H), 1.90 -1.78 (m, 4H); MS-ESI (m/z): 387 [M+H] +

4-(5-(4-chlorophenyl)-2-methyl-3-propionyl-1H-pyrrol-1-yl)benzenesulfonamide (A-867744):

A-867744 was synthesized using our modified synthetic route in one step from ethyl 5-(4-chlorophenyl)-2-methyl-1-(4-sulfamoylphenyl)-1H-pyrrole-3-carboxylate instead of reported four steps from the same intermediate1 (Faghih et al., 2009). Ethyl 5-(4-chlorophenyl)-2-methyl-1-(4-sulfamoylphenyl)-1H-pyrrole-3-carboxylate was synthesized by following the reported protocol from 2-bromo-1-(4-chlorophenyl)ethenone (Faghih et al., 2009) and used for the synthesis of A-867744 according to following procedure.

Ethyl 5-(4-chlorophenyl)-2-methyl-1-(4-sulfamoylphenyl)-1H-pyrrole-3-carboxylate (200 mg, 0.478 mmol) and N,O-dimethyl hydroxylamine (56 mg, 0.574 mmol) were dissolved with anhydrous THF in 100 ml flame dried two neck round bottom flask under argon atmosphere. The reaction mixture was cooled to 0˚C and ethylmagneisum bromide solution in THF was added dropwise to the reaction mixture. The reaction mixture was stirred at 0˚C for 30 min then quenched with saturated solution NH_4Cl. The aqueous layer was extracted with ethyl acetate, dried over Na_2SO_4, and concentrated under reduced pressure. The reaction mixture was purified by silica gel column chromatography to get pure desired compound A-867744 (39 mg, 21%).

1H NMR (CDCl3, 500 MHz): δ 7.98 (d, J=8.8 Hz, 2H), 7.28 (d, J=8.2 Hz, 2H), 7.17 (d, J=7.7 Hz, 2H), 8.95 (d, J=8.2 Hz, 2H), 6.74 (s, 1H), 4.89 (bs, 2H), 2.87 (q, J=7.1 Hz, 2H), 2.44 (s, 3H), 1.22 (t, J=7.1 Hz, 3 H); MS-ESI (m/z): 403 [M+H] +.

Chiral Separation of TQS:

Racemic TQS was synthesized as previously described (Gill et al., 2012). Since it was not known whether both isomers of TQS were active, we separated the isomers by preparative HPLC. Specifically, preparative Supercritical fluid chromatography was performed using a Chiralcel OD-H with super fluid and methanol (50/50) as a mobile phase at a 5.0 ml/min flow rate. Thus, from a 1.0 g batch of racemic TQS, we obtained 455 mg of the (-)-enantiomer 1a (SOR: -56.89; MeOH; c=0.450/100ml) and 455 mg of the (+)-enantiomer 1b (SOR: +61.75; MeOH; c=0.434/100ml).

Compound	Specific optical rotation
(-)-enantiomer 1a	-56.89; MeOH; c=0.450/100ml
(+)-enantiomer 1b	+61.75; MeOH; c=0.434/100ml

X-Ray analysis of TQS crystals

X-Ray Intensity data were collected at 100 K on a Bruker DUO diffractometer using MoKα radiation (λ = 0.71073 Å) and an APEXII CCD area detector. Raw data frames were read by program SAINT1 and integrated using 3D profiling algorithms. The resulting data were reduced to produce hkl reflections and their intensities and estimated standard deviations. The data were corrected for Lorentz and polarization effects, and numerical absorption corrections were applied based on indexed and measured faces.

The structure was solved and refined in SHELXTL2014, (Bruker-AXS, Madison, Wisconsin, USA) using full-matrix least-squares refinement. The non-H atoms were refined with anisotropic thermal parameters, and all of the H atoms were calculated in idealized positions and refined riding on their parent atoms. The correct stereochemistry

of the molecule is the one refined as confirmed by the low Flack x parameter of 0.007(9), determined by anomalous dispersion. All three protons on C2, C3, and C4 are syn to each other (lying on the same side of the average molecular plane). In the final cycle of refinement, 6884 reflections (of which 6242 are observed with $I > 2\sigma(I)$) were used to refine 256 parameters, and the resulting R1, wR2, and S (goodness of fit) were 3.85%, 10.22%, and 1.062, respectively. The refinement was carried out by minimizing the wR2 function using F2 rather than F values. R1 is calculated to provide a reference to the conventional R value but its function is not minimized.

Molecular modeling

The coordinates for the structure of α4β2 are from RCSB entry 6CNJ (Walsh et al., 2018). The energy minimization of small molecules in Figure 13 was done in ChemBio3D Ultra (PerkinElmer). Schrodinger Glide (Cambridge, MA) was used for docking.

Heterologous expression of nAChRs in Xenopus laevis oocytes

The human α9 clone, codon optimized for *Xenopus laevis,* was obtained from Veronika Grau and Katrin Richter (Giessen University, Giessen, Germany). Other human nAChR clones and concatamers were obtained from Dr. J. Lindstrom (University of Pennsylvania, Philadelphia, PA). The human resistance-to-cholinesterase 3 (RIC-3) clone, obtained from Dr. M. Treinin (Hebrew University, Jerusalem, Israel), was co-injected with α7 to improve the level and speed of α7 receptor expression without affecting the pharmacological properties of the receptors (Halevi et al., 2003). Subsequent to linearization and purification of the plasmid cDNAs, cRNAs were prepared using the mMessage mMachine in vitro RNA transfection kit (Ambion, Austin, TX). Site-directed mutants were made using the QuikChange kit (Agilent, Santa Clara CA) as previously described (Papke et al., 2011).

Oocytes were surgically removed from mature *Xenopus laevis* frogs (Nasco, Ft. Atkinson, WI) and injected with appropriate nAChR subunit cRNAs as described previously (Papke and Stokes, 2010). Frogs were maintained in the Animal Care Service facility of the University of Florida, and all procedures were approved by the University of Florida Institutional Animal Care and Use Committee. In brief, the frog was first anesthetized for 15-20 min in 1.5 L frog tank water containing 1 g of 3-aminobenzoate methanesulfonate buffered with sodium bicarbonate. The harvested oocytes were treated with 1.25 mg/ml collagenase (Worthington Biochemicals, Freehold, NJ) for 2 h at room temperature in calcium-free Barth's solution (88 mM NaCl, 1 mM KCl, 2.38 mM NaHCO3, 0.82 mM MgSO4, 15 mM HEPES, and 12 mg/l tetracycline, pH 7.6) to remove the follicular layer. Stage V oocytes were subsequently isolated and injected with 50 nl of 5-20 ng nAChR subunit cRNA. Recordings were carried out 1-7 days after injection.

Two-electrode voltage clamp electrophysiology

Experiments were conducted at room temperature (24°C) using OpusXpress 6000A (Molecular Devices, Union City, CA) (Papke and Stokes, 2010). Both the voltage and current electrodes were filled with 3 M KCl. Oocytes were voltage-clamped at -60 mV. The oocytes were bath-perfused with Ringer's solution (115 mM NaCl, 2.5 mM KCl, 1.8 mM CaCl2, 10 mM HEPES, and 1 μM atropine, pH 7.2) at 2 ml/min (α7 and α9) or at 4 ml/min (heteromeric). Drug applications were 12 s in duration followed by a 181 s washout period (α7 and α9) or 6 s in duration followed by a 241 s washout period (heteromeric). A typical recording for each oocyte constituted two initial control applications of ACh, an experimental compound applied alone or co-applied with ACh, and then follow-up control applications of ACh to determine primed potentiation of the ACh-evoked responses. The control ACh concentration was 30 μM unless otherwise indicated. The responses were calculated as both peak current amplitudes and net charge,

as previously described (Papke and Papke, 2002). The average responses of the two initial ACh controls from each cell were used for normalization. Statistical analyses were conducted based on T-test comparisons of the normalized net-charge data.

Data were collected at 50 Hz, filtered at 20 Hz (α7 and α9) or at 5 Hz (heteromeric), and analyzed by Clampfit 9.2 or 10.3 (Molecular Devices) and Excel (Microsoft, Redmond, WA). Data were expressed as means ± SEM from at least four oocytes for each experiment and plotted by Kaleidagraph 4.5.2 (Abelbeck Software, Reading, PA). Type II PAMs produce extremely large increases (>100,000-fold) in the single-channel currents of a small fraction of the receptors (≤ 1%), so they are intrinsically variable in amplitude and duration (Williams et al., 2011a), making it difficult to identify truly "representative" responses. Therefore, we display multi-cell averages for comparisons of these complex responses. The averages of normalized data were calculated using an Excel (Microsoft) template for each of the 10,500 points in each of the 210 s traces (acquired at 50 Hz). Following subtraction of the basal holding current, data from each cell, including the ACh controls, were normalized by dividing each point by the peak of the ACh control from the same cell. The normalized data were then averaged and standard errors of the mean (SEM) for the multi-cell averages calculated on a point-by-point basis. The dark lines represent the average normalized currents and the shaded areas the range of the SEM. Scale bars in the figures of averaged traces reflect the scaling factor relative to the average peak current amplitude of the ACh controls (con.) used for the normalization procedures. These plots are effectively augmented versions of typical bar plots of peak currents (Supplemental Figure 1) that additionally illustrate the differences in net charge, the kinetics of the responses, and the variability throughout the entire time course of the responses.

Results

Effects of L15'M mutations in receptors formed by the co-expression of α4 and β2

Cells expressing α4L15'M and β2L15'M were tested for their responses to applications of ACh applied alone or co-applied with the previously identified type II α7-PAMs, PNU-120596 (Hurst et al., 2005) or TQS (Gronlien et al., 2007). While the co-application of PNU-120596 had no effect on the ACh-evoked responses, 10 μM TQS produced a very large increase in the ACh-evoked responses ($p < 0.00001$ for peak current amplitudes), which did not readily return to baseline (Figure 2, see also Supplemental Figure 1).

Impact of L15'M mutations in α4 and β2, alone or in combination

We evaluated the impact of the L15'M mutations in either or both subunits of α4β2 receptors compared to responses of receptors formed with wild-type subunits. All groups of cells were injected on the same day and tested 7 days after injection. The control ACh peak current responses of cells with either the α4L15'M mutation (α4∗β2) or the β2L15'M mutation (α4β2∗) were less than wild-type α4β2 ACh responses ($p < 0.05$) but still reasonably robust. However, the ACh control responses of the double mutants (α4∗β2∗) were severely compromised compared to wild-type ($p < 0.001$), reduced to only about 5% of wild-type control responses (Figure 3A).

Responses to ACh plus 10 μM TQS compared to ACh alone in the same cells were greatly increased in cells containing β2L15'M subunits ($p < 0.001$), regardless of whether the mutant β subunit was co-expressed with wild-type α4 or α4L15'M. The relative potentiation of the double mutant α4∗β2* was larger ($p < 0.05$) than that of the α4β2∗ receptors (Figure 3B). However, comparison of the TQS-potentiated responses of the mutant receptors that were normalized to the average responses of the wild-type receptors recorded on the same day (Figure 3C), indicated that the apparent large

JPET Fast Forward. Published on June 7, 2019 as DOI: 10.1124/jpet.119.259499
This article has not been copyedited and formatted. The final version may differ from this version.

potentiation of the double mutants was due to the negative effect on ACh-evoked responses by the mutations in the α subunits (Figure 3A); this limitation was partly reversed by TQS when mutant β subunits were also present. The raw data shown in Figure 3D clearly shows that the presence of the L15'M mutation in β2 was necessary for TQS to potentiate ACh-evoked responses, while the mutation in α4 alone had no effect on TQS sensitivity.

In addition to potentiating responses evoked by ACh or other orthosteric agonists, type II PAMs will also reactivate receptors previously desensitized (Papke et al., 2009; Williams et al., 2011a). We used an application of 30 μM nicotine to desensitize α4β2L15M receptors. In a separate experiment we determined that this concentration of nicotine reduced subsequent control ACh responses by 55% compared to initial controls ($p < 0.01$ $n = 8$) and that ACh responses showed no significant recovery over the course of three ACh applications (not shown). Under these conditions, where a large fraction of the α4β2L15'M receptors were unresponsive to ACh, we applied 1 μM TQS alone and determined that the addition of TQS was sufficient to draw receptors out of desensitization and back into activated states (Figure 3E).

ACh and TQS concentration-response studies of α4β2L15'M receptors

The co-expression of α4 and β2 subunits can potentially result in receptors with different subunit stoichiometry, α4(3)β2(2) or α4(2)β2(3) (Nelson et al., 2003), and unless influenced by the ratio of RNAs injected or constrained by the use of subunit concatamers (Zhou et al., 2003), mixed populations of receptors may be observed. When receptors are constrained to adopt the so-called high-sensitivity (HS) α4(2)β2(3) configuration, ACh response curves achieve maximum values at about 10 μM, and higher concentrations of ACh evoke no larger responses. The alternative low-sensitivity (LS) α4(3)β2(2) configuration tends to generate larger currents more rapidly after injection, and, due to the presence of a low-affinity ACh site at the α4–α4 interface

(Harpsoe et al., 2011; Lucero et al., 2016), these receptors show increasing responses to ACh across a larger range of concentrations. Based on a two-site curve fit (Supplemental Figure 2, Supplemental Table 1), the receptors resulting from the co-injection of α4 with β2L15'M appeared to form mostly (≈88%) HS-type receptors with an EC_{50} of 3 μM but with a significant (≈10%) LS component with an EC_{50} of 281 μM (Figure 4A). This suggests that most of the receptors resulting from the co-injection of α4 wild-type and mutant β2 had three mutant subunits per receptor.

The potentiation of 30 μM ACh responses by TQS (Figure 4B) showed an EC_{50} of 1.8 ± 0.3 μM and an E_{max} for the potentiation of peak currents of 13.6 ± 0.8-fold, relative to ACh alone. However, it should be noted that this efficacy estimate, based on the measurement of peak current, is clearly an underestimate of the overall effect of TQS on receptor activation. As shown in Figure 4C, co-application of ACh and TQS, especially at concentrations ≥ 3 μM, resulted in protracted responses that did not return to baseline even after several minutes of washout.

Evaluation of the TQS analog, the ago-PAM GAT107

TQS has proven to be a valuable scaffold for the development of analogs with diverse properties (Gill-Thind et al., 2015; Horenstein et al., 2016), including 4BP-TQS (Gill et al., 2011) and its active isomer, GAT107 (Papke et al., 2014). While typical PAMs require co-application with an orthosteric agonist, ago-PAMs appear to work at two sites, the transmembrane site controlled by the α7M15' residue and an allosteric activation site in the extracellular domain (Horenstein et al., 2016; Gulsevin et al., 2019). We evaluated the activity of the ago-PAM GAT107 on cells expressing α4 and β2L15'M (Figure 5). We observed a relatively small but significant ($p < 0.01$) increase in ACh responses when 10 μM GAT107 was co-applied with ACh (Figure 5A). We observed no allosteric activation when GAT107 was applied alone; however, there was a small

JPET Fast Forward. Published on June 7, 2019 as DOI: 10.1124/jpet.119.259499
This article has not been copyedited and formatted. The final version may differ from this version.

residual (primed) potentiation ($p < 0.05$) of an ACh response after the application of GAT107 alone (Figure 5B).

The selectivity of stereoisomers for the potentiation α4β2L15'M receptors

Although the selectivity of stereoisomers has not been well investigated for most α7 PAMs, as noted above, 4BP-TQS can be separated into active (GAT107) and inactive isomers (GAT106) (Thakur et al., 2013). We confirmed that the 4BP-TQS isomer that lacked activity on α7 was likewise inactive on α4β2L15'M receptors (Figure 5C).

We prepared the corresponding isomers of TQS and determined that the active isomer was (-)-TQS (Figure 5D). (-)-TQS was very active on both α4β2L15'M and α7, producing robust potentiation at sub-micromolar concentrations, greater than was typically observed with the racemic preparation (Figure 4), suggesting that the presence of the (+) isomer might actually limit the responses to racemic TQS. To test this, we co-applied ACh with 300 nM (-)-TQS alone or with 3 μM (+)-TQS and confirmed that the inactive isomer functions as an antagonist of (-)-TQS (Figure 5D).

The X-ray crystal structure of (-)-TQS is shown in Figure 5E. The key stereo chemical features of GAT107, which is the active enantiomer of 4-BP-TQS, are the same in the active TQS isomer (Figure 5F). The structural differences that must account for the differences in the relative efficacy of these molecules for α7 and PAM-sensitive heteromeric receptors are highlighted in the overlay.

Evaluations of additional PAMs

We determined that A-867744 (Faghih et al., 2009), an α7 PAM previously suggested to have a different mechanism of action compared to others (Newcombe et al., 2018), also had significant potentiating effects on α4β2L15'M receptors; peak current responses to 30 μM ACh were increased by a factor of 5.1 ± 0.6-fold with co-application of A-867744. The ago-PAM B-973B (Post-Munson et al., 2017) had neither agonist nor

JPET Fast Forward. Published on June 7, 2019 as DOI: 10.1124/jpet.119.259499
This article has not been copyedited and formatted. The final version may differ from this version.

PAM activity on α4β2L15'M receptors (not shown). Noting the structural difference between GAT107 and TQS (Figure 5), we tested an alternative PAM, GAT927 (Figure 6), which like TQS has a double ring structure at the base. Similar to effects of ago-PAMs on α7, GAT927 was able to activate α4β2L15'M receptors when applied alone (Figure 6A), and this relatively modest allosteric activation was followed by a prolonged period of primed potentiation of subsequent ACh-evoked responses (Papke et al., 2014). The potency and efficacy of GAT927 for α4β2L15'M receptors was so great that it could only be characterized across a limited range of concentrations. Although the allosteric activation produced by concentrations of GAT927 up to 300 μM could be measured (Figure 6B), responses to ACh following the application of GAT927 alone at concentrations ≥ 30 μM were too large to voltage clamp. Likewise, responses to ACh co-applied with GAT927 concentrations ≥ 30 μM were too large to voltage clamp (Figure 6C).

Potentiating effects of GAT927 on α4β2 receptors with varying numbers of β2L15'M subunits

Using linked α4β2 subunits (Zhou et al., 2003) with or without the β2L15'M mutation and co-expressing them with wild-type β2 or β2L15'M, we were able to constrain the receptor composition to contain zero, one, two, or three mutant subunits (Figure 7A). Comparing the responses of cells that were all injected at the same time, we determined that ACh control responses for receptors with multiple β2 mutant subunits were significantly reduced compared to wild-type controls ($n \geq 5$, $p < 0.001$), similar to the effect of the L15'M mutation in the α4 subunits (Figure 7B). The presence of the mutation in the single β subunit in the accessory subunit position (outside the ACh binding sites) (Nelson et al., 2003) produced no significant effect on the amplitude of ACh control responses. While the relative effect of 3 μM GAT927 co-application with ACh to receptors with two or three mutant subunits was greater than the relative effects

JPET Fast Forward. Published on June 7, 2019 as DOI: 10.1124/jpet.119.259499
This article has not been copyedited and formatted. The final version may differ from this version.

on receptors with a single mutant subunit (Figure 7C), this appeared to be largely a relief of the effects of multiple mutants on basic ACh-evoked responses. The absolute magnitudes of the potentiated responses were not significantly different regardless of the number of mutant β subunits (Figure 7D). Additionally, the receptors with single mutant β subunits showed more pronounced prolonged potentiation of subsequent ACh-evoked responses (Figure 7 E and F).

To confirm that a single mutant β subunit would be sufficient to make receptors sensitive to α7 PAMs regardless of its position within the receptor, the alternative concatamer α4–6–β2 (Zhou et al., 2003) was co-expressed with the L15'M β2 mutant. This combination is also expected to produce receptors with a single mutant β; however, in this case the mutant would be in one of the two ACh binding site beta subunits, and the beta in the accessory subunit would be wild-type. The control responses of these cells to 30 μM ACh were 280 ± 3 nA (n = 7), and the co-application of 10 μM TQS with 30 μM evoked responses that were 10.1 ± 3.4-fold larger than ACh alone ($p < 0.001$, not shown). While the presence of a β2L15'M subunit in the accessory subunit position did not significantly impact the amplitude of ACh controls, receptors formed by the co-expression of β2L15'M with the alternative concatamer α4–6–β2 had compromised ACh control responses ($p < 0.05$, n = 8). Average peak responses were 162 ± 19 nA when the concatamer was co-expressed with wild-type β2, and 97 ± 15 nA when co-expressed with β2L15'M.

We also tested the impact of multiple L15'M mutations in receptors constrained to have the LS α4(3)β2(2) configuration and obtained results consistent with the HS receptor results shown in Figure 7 (Supplemental Figure 3). Note that in order to form these receptors, we used the concatamer that places a β2L15'M in each of the ACh binding sites, and that the receptors with one or three mutations incorporated α4L15'M subunits. All of these receptors had reduced ACh control responses, and those with two β2L15'M subunits were potentiated by 10 μM TQS. The receptors with two β2L15'M

JPET Fast Forward. Published on June 7, 2019 as DOI: 10.1124/jpet.119.259499
This article has not been copyedited and formatted. The final version may differ from this version.

subunits that lacked α4L15'M were potentiated by the relatively low concentration of TQS used (10 μM) only to a level equivalent to the wild-type control.

Since the location of a single mutant β2 subunit in the accessory subunit position (Figure 7) was sufficient to produce potentiation without a decrease in ACh control responses, we tested the ACh concentration responses of α4(2)β2(2)β2L15'M receptors alone or in the presence of a fixed concentration of TQS to determine the degree that TQS affected ACh potency (Supplemental Figure 4, Supplemental Table 2). TQS produced both a four-fold increase in I_{max} and a three-fold decrease in the ACh EC_{50}.

Effect of the number of M15'L mutants in a7

The data with α4β2 receptors indicated that the greater the number of L15'M subunits present, the smaller the amplitude of control ACh responses (Figure 7B). We expressed RNA coding for wild-type α7 and α7M254L alone or at varying ratios to determine whether reducing the number of L15'M subunits would increase ACh control responses. We saw no significant difference in the ACh control responses over a wide range of subunit ratios (Figure 8). The potentiating effects of 1 μM TQS were less compared to wild-type α7 if the wild-type RNA was less that 50%.

Evaluation of HS and LS α4β2 analogs with β2L15'M in the binding sites and wild-type α4 or β2 in the accessory subunit position

The β2L15'M–6–α4 concatamer was co-expressed with either wild type α4 or β2 to yield LS or HS forms of α4β2, respectively, with the L15'M mutation in the two β subunits that contribute to the ACh binding sites. As expected, the LS analogs had larger ($p < 0.05$) responses to 100 μM ACh (Figure 9A). Also, as expected, due to the low affinity α4–α4 binding site, LS receptors had a large increase in response to 100 μM ACh compared to 10 μM ACh ($p < 0.01$), while the HS analogs showed no increase in response at 100 μM compared to 10 μM (Figure 9B). The LS analogs were potentiated

JPET Fast Forward. Published on June 7, 2019 as DOI: 10.1124/jpet.119.259499
This article has not been copyedited and formatted. The final version may differ from this version.

about 3-fold by TQS, while the normalized potentiation of HS receptors was 24-fold (Figure 9C); however, the potentiated LS responses were larger ($p < 0.05$) than potentiated HS receptors in absolute magnitude (Figure 9D).

The relative potentiation of α4β2$_{L15'M}$ and α7 by select PAMs

We determined the relative activity of TQS, GAT927, and other published PAMs for these α4β2$_{L15'M}$ and α7 receptors (Figure 10). Consistent with the fact that PNU-120596, a very active α7 PAM, failed to potentiate α4β2L15'M receptors, the data indicate that the structure-activity relationship proscribed by the PAM binding sites in these two receptor types differs remarkably. As noted previously, GAT107 was relatively ineffective on the α4β2$_{L15'M}$ receptors, while GAT927 was much more active ($p < 0.001$) on α4β2$_{L15'M}$ receptors than α7 receptors.

The effect of β2L15'M co-expression with alternative α subunits

Initial studies of neuronal nAChR subtype expression indicated that heteromeric receptors could be formed with various combinations of α and β subunits. The β2 subunits readily form receptors when co-expressed with α2 or α3 (Boulter et al., 1987; Wada et al., 1988; Papke et al., 1989) and will additionally substitute to a certain degree for the muscle β1 subunit (Papke, 2014). TQS-sensitive receptors were formed when β2L15'M was co-expressed with either α2 or α3 (Figure 11).

We also co-expressed wild-type β2 or β2L15'M with an α2/β2 concatamer (β2−6−α2) (Papke et al., 2013) that, like the β2−6−α4 concatamer in Figure 7, would put a single mutant β2 in the accessory position. When the receptors contained the single β2L15'M subunit, co-application of 10 μM TQS produced a 23.7 ± 2.1 -fold increase in ACh-evoked responses ($p < 0.0001$, $n = 6$). As was the case with the α4-containing receptors, (Figure 7), ACh control responses were not significantly reduced with the

mutant β2 subunit in the accessory position. Responses to 10 μM ACh were 120 ± 11 nA with a wild-type β2 (n = 8) and 101 ± 16 nA with β2L15'M.

TQS sensitivity of receptors formed with a β4L15'M subunit

We made the corresponding L15'M mutation in the alternative neuronal β subunit, β4 (Duvoisin et al., 1989). As shown in Figure 12, the receptors formed with any of the three neuronal α subunits tested showed significant potentiation ($p < 0.01$) when ACh was co-applied with 10 μM TQS. The relative potentiation was less ($p < 0.05$) than was obtained with β2L15'M co-expression, although it is interesting to note that there was protracted activation of the receptors formed with α4 and β4L15'M subunits, similar to what was observed with α4 and β2L15'M subunits (Figure 4).

Impact of 15'M mutations in other nAChR

We made the corresponding L15'M mutation in the muscle β1 subunit; however, the co-expression of β1L15'M with α1, ε, and δ resulted in cells that were unresponsive to ACh alone or co-applied with either TQS or GAT927 (not shown). However, a number of interesting effects were observed when the L15'M mutation was placed in the other muscle subunits, summarized in Table 1. Cells were from the same batch of oocytes and tested just 1 day after injection. Surprisingly, ACh control responses were significantly larger than wild-type receptors if the mutation was in the γ or δ subunits. However, for all subunit combinations tested that had the L15'M mutation in any subunit, co-application of 10 μM TQS produced a significant reduction in ACh responses (Table 1).

The sequence of α9 and α10 at the 15' position is unique from α7 and other nAChR, being a glutamine (Q) rather than either L or M (Figure 1). The expression of α9 in oocytes is relatively inefficient (Verbitsky et al., 2000); however, in our hands α9 expression has been significantly improved with a version of α9 that has been codon

optimized for *Xenopus* (Zakrzewicz et al., 2017). We mutated the 15' residue in the codon-optimized α9 clone to either L or M. Tested 5 days after injection, cells expressing the wild-type α9 gave peak current responses to 300 μM ACh and 3 mM choline of 1.44 ± 0.53 and 0.38 ± 0.11 μA, respectively (n = 6). As expected, responses to 300 μM ACh were not increased by co-application with 10 μM TQS. However, there were no detectable responses of either α9Q15'L or α9Q15'M to 300 μM ACh with or without 10 μM TQS (not shown).

Receptors containing α5L15'M

The α5 subunit does not form typical ACh binding sites when co-expressed with other nAChR subunits but will take the position of the accessory subunit when co-expressed with the β2−6−α4 concatamer (Kuryatov et al., 2008). We engineered the L15'M mutation into α5 and co-expressed it with the concatamer. The effects of the mutation in this receptor were rather subtle. Not surprisingly, compared to α4(2)β2(2)α5 receptors from the same injection set, the ACh control responses of receptors with the α5L15'M subunit were significantly ($p < 0.05$) smaller those with the wild-type α5 (165 ± 19 nA compared to 710 ±195 nA, n = 7 in each group). However, there was only a very slight potentiating effect ≈ 20% ($p < 0.05$) when ACh was co-applied with 10 μM TQS. We then tested the α4(2)β2(2)α5L15'M receptors with a co-application of 30 μM GAT927 and noted that the peak currents of the co-application responses were 3.73 ± 0.66 that of the ACh controls (n = 6, not shown). Note, however, this relatively small but significant ($p < 0.05$) effect did no more than bring the level of the mutant's potentiated responses up to the level of the ACh controls of the receptors without the L15'M mutation in the α5 subunit.

JPET Fast Forward. Published on June 7, 2019 as DOI: 10.1124/jpet.119.259499
This article has not been copyedited and formatted. The final version may differ from this version.

α7 PAM binding sites in α4β2$^{L15'M}$ receptors

At present the best available models of α7 structure (Li et al., 2011; Nemecz and Taylor, 2011) are homology models based on mutant forms of the AChBP and do not include any of the transmembrane or intracellular domains. Attempts to model the PAM binding site have therefore had to rely on relatively low-resolution structures such as those extrapolated from a *Torpedo* nAChR cryomicroscopy density map (Newcombe et al., 2018). We instead analyzed mutation data in the context of experimental high-resolution structural information (Figure 13A), where side chain positions are not ambiguous (Walsh et al., 2018). As predicted by the sequence data (Figure 1), the L/M site (residue 254 in α7) is toward the extracellular end of the pore-forming TM2, while the alternative site, A226, previously shown to be important for PNU-120596 potentiation of α7, is deep within the transmembrane region on TM1 (Young et al., 2008). Also shown in the figure are the structures of PNU-120596 and the TQS isomers at the same scale. We attempted to dock the (-)-TQS molecule into this structure. However, docking to the cryo-EM structure of the α4β2 receptor in complex with the agonist nicotine did not reveal a high affinity binding site for TQS. This result suggests that the receptor requires a conformational change in order to create such a pocket and bind TQS with high affinity. Additionally, we hypothesize that the L15'M mutation is likely to engender a specific reorganization that is not represented in the cryo-EM structure. Moreover, the structure shown is presumed to represent a desensitized state (Walsh et al., 2018), and a primary effect of the binding of the TQS analogs would be to destabilize desensitized conformations.

PNU-120596 and TQS are roughly the same size, potentially large enough to span the distance between L255 and A227 (β2 numbering). The original data identifying these residues (Young et al., 2008) was based only on the use of PNU-120596. In β2L15'M, both of these residues are the same as in α7 wild-type, but the α4β2L15'M receptors are insensitive to PNU-120596. We therefore tested whether L254 and A226 residues

differentially affected TQS and PNU-120596 activity in α7 (Figure 13B). Our data confirmed that both of these residues profoundly reduce the potentiating activity of PNU-120596 but indicated that TQS potentiation is insensitive to the A226D mutation. These data suggest that the binding or coupling mechanisms for these two PAMs differ in α7 and that some structural elements unique to the neuronal beta mutants are permissive for TQS potentiation but restrict PNU-120596 from being active, and account for the differing structure-activity relationships shown in Figure 10. Of course, since PAM binding and/or the coupling of binding to facilitated channel activation, are likely to involve interactions between subunits, crucial structural elements may also be present in the complementary subunits at the subunit-subunit interfaces.

Discussion

The α7 nAChR has an intrinsically low probability of opening (P_{open}) immediately after a large jump in ACh concentration or in the sustained presence of agonist (Williams et al., 2012). This is largely due to a form of desensitization that is unique to α7 and induced by high levels of ACh binding site occupancy (Papke and Papke, 2002; Uteshev et al., 2002). This special form of desensitization can be destabilized by type II PAMs (Gronlien et al., 2007), which are selective for α7 wild-type receptors (Williams et al., 2011a; Williams et al., 2011b). In contrast, muscle-type and heteromeric neuronal nAChR have a very high P_{open} immediately after a large jump in ACh concentration (Li and Steinbach, 2010) but then transition to an equilibrium condition that favors desensitized conformations (Campling et al., 2013). Studies of mutants and chimeras between α7 and the structurally related, but PAM-insensitive, homomeric 5HT3A receptor identified several residues within the α7 transmembrane domain (Figure 1) that were required for the activity of the PAM PNU-120596 (Bertrand et al., 2008; Young et al., 2008). It has been proposed that these residues define a binding site that accommodates the PAM (Newcombe et al., 2018), although it is equally

possible that at least some of these residues were required not for PAM binding per se but for the coupling between the agonist binding sites and the channel gating domains.

The type II PAMs like PNU-120596 and TQS are distinguished from other less efficacious type I PAMs because of their ability to reverse receptor desensitization (Gronlien et al., 2007). Interestingly, their effects appear to produce extremely large increases in the P_{open} of a relatively small percentage of channels at any given time (Williams et al., 2011a; Andersen et al., 2016). The relationship between macroscopic and single-channel current is dependent on three factors: N (total number of receptors contributing to the response), P_{open}, and γ (single channel conductance). When studying the currents of a single channel, by definition, N is equal to one, and for such single-channel currents in the presence of a PAM like PNU-120596 or an ago-PAM like GAT107, the increase in P_{open} is on the order of one hundred thousand or more, while the macroscopic effect of such PAMs is perhaps a thousand-fold lower, suggesting a proportionally smaller number of receptors contributing to the macroscopic (whole cell) response (Williams et al., 2011a).

Examination of the putative PAM binding domain in α7 highlights the unique methionine in the 15' position of TM2 (Figure 1), one of the two most important residues for PAM activity identified by site-directed mutations (Young et al., 2008). This position could be mutated in α7 to L without apparent change in function except in regard to PAM activity. We see neither a change in amplitude nor kinetics of macroscopic current in α7M254L compared to wild-type. In contrast, when the reverse mutation was made in $\alpha4\beta2$ receptors, we saw large decreases in the control responses to ACh when one or more subunits in the ACh binding sites contained a 15'M subunit (Figures 3 & 7). In the case of the α4L15'M mutants, this was the only effect we observed (Figure 3), while when the mutation was present in β2 subunits, we saw that receptors became sensitive to a number of PAMs previously reported to be selective for α7 (Figures 5-7).

As noted above, macroscopic responses are determined by three factors, N, P_{open}, and γ. It is plausible that a 15' M residue in subunits that form agonist binding sites could affect receptor assembly or trafficking, but it seems more likely that it affects the coupling of agonist binding to channel activation and hence P_{open}, especially since PAMs can bring up the currents in receptors containing multiple mutant subunits to levels equivalent to or greater than wild-type receptors (i.e. compensating for decreased control ACh response). Simply because methionine is much more flexible than leucine, the mutation could result in a less stable interface among the TM helices at this position, destabilizing the allosteric network important for gating. The fact that the decreases in macroscopic currents require the presence of the mutation in an agonist binding subunit would also seem to make an effect on gating most likely. However, the methionine side chain is also longer than that of leucine, and by steric repulsion may 'push' the apical portion of M2 more toward the pore axis, making it harder to fully open the channel, which would suggest a possible decrease in γ.

The effects of the L15'M mutation seem to be consistent for all of the common functional neuronal α/β heteromeric receptors (Figures 11 & 12), where α is α2, α3, or α4, and β is β2 or β4. It is reasonable to hypothesize that, as in α7 receptors, the PAM's effect on these receptors enables a bursting state coupled to what would otherwise be a desensitized form of the receptor. This, as well as a direct determination of whether there are changes in single-channel conductance, will be a focus of future single-channel studies.

The β2L15'M subunit itself may prove to be a useful experimental tool. However, while in our in vitro system we can limit the expression of the β2 mutant to the accessory subunit and thus avoid the effect of reducing P_{open} in the absence of a PAM, in vivo the mutation would necessarily be in all β subunits. Therefore, the expression of β2L15'M in β2−knockout animals would allow for only a partial rescue of function. However, the delivery of a PAM, especially one as efficacious as GAT927, would

perhaps produce a significant gain of function, amplifying the function of β2-containing receptors for behaviors such as nicotine self-administration. Additionally, the identification of PAM-sensitive heteromeric nAChR provides new opportunities to study the basis for α7 nAChR receptor dynamics in a system that is arguably both more simple and more complex.

α7 nAChR have long been considered interesting targets for therapeutics, beginning with the identification of GTS-21 as a selective partial agonist (Papke et al., 1996). Although no α7 agonists have passed the rigors of clinical trials, their utility has been supported by many preclinical studies (Leiser et al., 2009; Wallace et al., 2011; Prickaerts et al., 2012; Bertrand et al., 2015; Pieschl et al., 2017). More recently, with the discovery of α7's role in CAP (Pavlov et al., 2007; Rosas-Ballina et al., 2009; Rosas-Ballina and Tracey, 2009), α7 drugs continue to be investigated as alternative analgetic agents for inflammatory and neuropathic pain (Bagdas et al., 2017). The discovery of α7 PAMs have further enlarged these potentially important therapeutic directions. Interestingly, although the activity on the immune cells that mediate CAP does not seem to require α7 channel activation (Papke et al., 2015), the α7 PAMs PNU-120596 (Freitas et al., 2013) and TQS (Abbas et al., 2017) have both been shown to have CAP activity.

Many challenges remain for understanding α7 as a therapeutic target, including the definition of its complex conformational dynamics and how those dynamics may couple to intracellular signal transduction (Kabbani and Nichols, 2018). The structure-activity relationship for PAM activity on α4β2L15'M receptors is quite different from α7, based on both the inactivity of some PAMs (e.g. PNU-120596) on α4β2L15'M receptors and the relative activity of TQS analogs that are active on both. While there are at present no actual α7 structures that incorporate the putative PAM binding site, the cryo-EM structure of α4β2 receptors offers a promising new approach for studying the allosteric modulation of nAChR, especially if new structures can be generated of α4β2 receptors including the 15' mutation with TQS in situ.

Additionally, our studies refute the hypothesis that PAMs like TQS were selective for α7 because they reversed the form of desensitization that was a unique limiting factor to α7-mediated currents (Williams et al., 2012) and suggest that, rather, they can reverse forms of desensitization common to all nAChR. The phenomenon of desensitization, since first described by Katz and Thesleff (Katz and Thesleff, 1957) for muscle-type nAChR, has been "an elephant in the room" for all subsequent studies of nAChR. The role of α4β2 desensitization in reinforcing effects of nicotine remains a contentious subject (Picciotto et al., 2008). By identifying a new tool for studying α4β2 desensitization, we may ultimately gain more understanding of nicotine addiction, which in the case of cigarette smoking is the single most preventable cause of death in many countries.

Acknowledgements

The authors thank Lu Wenchi Corrie for care and diligence in the performance of the oocyte experiments. KAA wishes to acknowledge the National Science Foundation and the University of Florida for funding of the purchase of the X-ray equipment.

Authorship contributions

Participated in research design: Stokes and Papke

Conducted experiments: Stokes and Abboud

Contributed new reagents or analytic tools: Garai, Kulkarni, Cantwell, Noviello, and Thakur

Performed data analysis: Papke

Wrote or contributed to the writing of the manuscript: Stokes, Noviello, Thakur, Hibbs, Horenstein, and Papke

References

Abbas M, Alzarea S, Papke RL and Rahman S (2017) The alpha7 nicotinic acetylcholine receptor positive allosteric modulator attenuates lipopolysaccharide-induced activation of hippocampal IkappaB and CD11b gene expression in mice. *Drug Discov Ther* **11**:206-211.

Akabas MH, Kaufmann C, Archdeacon P and Karlin A (1994) Identification of acetylcholine receptor channel-lining residues in the entire M2 segment of the alpha subunit. *Neuron* **13**:919-927.

Andersen ND, Nielsen BE, Corradi J, Tolosa MF, Feuerbach D, Arias HR and Bouzat C (2016) Exploring the positive allosteric modulation of human alpha7 nicotinic receptors from a single-channel perspective. *Neuropharmacology* **107**:189-200.

Bagdas D, Gurun MS, Flood P, Papke RL and Damaj MI (2017) New Insights on Neuronal Nicotinic Acetylcholine Receptors as Targets for Pain and Inflammation: A Focus on alpha7 nAChRs. *Curr Neuropharmacol*.

Bagdas DA, Wilkerson JL, Kulkarni A, Toma W, AlSharari S, Gul Z, Lichtman AH, Papke RL, Thakur GA and Damaj MI (2016) The alpha7 nicotinic receptor dual allosteric agonist and positive allosteric modulator GAT107 reverses nociception in mouse models of inflammatory and neuropathic pain. *Br J Pharm* **173**:2506-2520.

Bertrand D, Bertrand S, Cassar S, Gubbins E, Li J and Gopalakrishnan M (2008) Positive allosteric modulation of the alpha7 nicotinic acetylcholine receptor: ligand interactions with distinct binding sites and evidence for a prominent role of the M2-M3 segment. *Mol Pharmacol* **74**:1407-1416.

Bertrand D, Lee CH, Flood D, Marger F and Donnelly-Roberts D (2015) Therapeutic Potential of alpha7 Nicotinic Acetylcholine Receptors. *Pharmacol Rev* **67**:1025-1073.

Boulter J, Connolly J, Deneris E, Goldman D, Heinemann S and Patrick J (1987) Functional expression of two neural nicotinic acetylcholine receptors from cDNA clones identifies a gene family. *Proc Natl Acad Sci USA* **84**:7763-7767.

Campling BG, Kuryatov A and Lindstrom J (2013) Acute activation, desensitization and smoldering activation of human acetylcholine receptors. *PLoS One* **8**:e79653.

Clarke PBS, Schwartz RD, Paul SM, Pert CB and Pert A (1985) Nicotinic binding in rat brain: autoradiographic comparison of [^{3}H] acetylcholine [$_{3}$H] nicotine and [^{125}I]-alpha-bungarotoxin. *J Neurosci* **5**:1307-1315.

Duvoisin RM, Deneris E, Patrick J and Heinemann S (1989) The functional diversity of the neuronal acetylcholine receptors is increased by a novel subunit: b4. *Neuron* **3**:487-496.

Elgoyhen AB, Vetter DE, Katz E, Rothlin CV, Heinemann SF and Boulter J (2001) alpha10: a determinant of nicotinic cholinergic receptor function in mammalian vestibular and cochlear mechanosensory hair cells. *Proc Natl Acad Sci U S A* **98**:3501-3506.

Faghih R, Gopalakrishnan SM, Gronlien JH, Malysz J, Briggs CA, Wetterstrand C, Ween H, Curtis MP, Sarris KA, Gfesser GA, El-Kouhen R, Robb HM, Radek RJ, Marsh KC, Bunnelle WH and Gopalakrishnan M (2009) Discovery of 4-(5-(4-chlorophenyl)-2-methyl-3-propionyl-1H-pyrrol-1-yl)benzenesulfonami de (A-867744) as a novel positive allosteric modulator of the alpha7 nicotinic acetylcholine receptor. *J Med Chem* **52**:3377-3384.

Freitas K, Ghosh S, Ivy Carroll F, Lichtman AH and Imad Damaj M (2013) Effects of alpha7 positive allosteric modulators in murine inflammatory and chronic neuropathic pain models. *Neuropharmacology* **65**:156-164.

Garai S, Raja KS, Papke RL, Deschamps JR, Damaj MI and Thakur GA (2018) B-973, a Novel alpha7 nAChR Ago-PAM: Racemic and Asymmetric Synthesis,

Electrophysiological Studies, and in Vivo Evaluation. *ACS Med Chem Lett* **9**:1144-1148.

Gill JK, Dhankher P, Sheppard TD, Sher E and Millar NS (2012) A series of alpha7 nicotinic acetylcholine receptor allosteric modulators with close chemical similarity but diverse pharmacological properties. *Mol Pharmacol* **81**:710-718.

Gill JK, Savolainen M, Young GT, Zwart R, Sher E and Millar NS (2011) Agonist activation of alpha7 nicotinic acetylcholine receptors via an allosteric transmembrane site. *Proc Natl Acad Sci U S A* **108**:5867-5872.

Gill-Thind JK, Dhankher P, D'Oyley JM, Sheppard TD and Millar NS (2015) Structurally similar allosteric modulators of alpha7 nicotinic acetylcholine receptors exhibit five distinct pharmacological effects. *J Biol Chem* **290**:3552-3562.

Gronlien JH, Haakerud M, Ween H, Thorin-Hagene K, Briggs CA, Gopalakrishnan M and Malysz J (2007) Distinct profiles of alpha7 nAChR positive allosteric modulation revealed by structurally diverse chemotypes. *Mol Pharmacol* **72**:715-724.

Gulsevin A, Papke RL, Stokes C, Garai S, Thakur GA, Quadri M and Horenstein N (2019) Allosteric agonism of alpha7 nicotinic acetylcholine receptors. *Mol Pharmacol*.

Halevi S, Yassin L, Eshel M, Sala F, Sala S, Criado M and Treinin M (2003) Conservation within the RIC-3 gene family. Effectors of mammalian nicotinic acetylcholine receptor expression. *J Biol Chem* **278**:34411-34417.

Harpsoe K, Ahring PK, Christensen JK, Jensen ML, Peters D and Balle T (2011) Unraveling the high- and low-sensitivity agonist responses of nicotinic acetylcholine receptors. *J Neurosci* **31**:10759-10766.

Hone AJ, Servent D and McIntosh JM (2018) alpha9-containing nicotinic acetylcholine receptors and the modulation of pain. *Br J Pharmacol* **175**:1915-1927.

Horenstein NA, Papke RL, Kulkarni AR, Chaturbhuj GU, Stokes C, Manther K and Thakur GA (2016) Critical molecular determinants of alpha7 nicotinic acetylcholine receptor allosteric activation: separation of direct allosteric activation and positive allosteric modulation. *J Biol Chem* **291**:5049-5067.

Hurst RS, Hajos M, Raggenbass M, Wall TM, Higdon NR, Lawson JA, Rutherford-Root KL, Berkenpas MB, Hoffmann WE, Piotrowski DW, Groppi VE, Allaman G, Ogier R, Bertrand S, Bertrand D and Arneric SP (2005) A novel positive allosteric modulator of the alpha7 neuronal nicotinic acetylcholine receptor: in vitro and in vivo characterization. *J Neurosci* **25**:4396-4405.

Kabbani N and Nichols RA (2018) Beyond the Channel: Metabotropic Signaling by Nicotinic Receptors. *Trends Pharmacol Sci* **39**:354-366.

Katz B and Thesleff S (1957) A study of the "desensitization" produced by acetylcholine at the motor end-plate. *Journal of Physiology (London)* **138**:63-80.

Kulkarni AR and Thakur GA (2013) Microwave-assisted Expeditious and Efficient Synthesis of Cyclopentene Ring-fused Tetrahydroquinoline Derivatives Using Three-component Povarov Reaction. *Tet Let* **54**:6592-6595.

Kuryatov A, Onksen J and Lindstrom J (2008) Roles of accessory subunits in alpha4beta2(*) nicotinic receptors. *Mol Pharmacol* **74**:132-143.

Leiser SC, Bowlby MR, Comery TA and Dunlop J (2009) A cog in cognition: how the alpha7 nicotinic acetylcholine receptor is geared towards improving cognitive deficits. *Pharmacol Ther* **122**:302-311.

Levin ED and Rezvani AH (2000) Development of nicotinic drug therapy for cognitive disorders. *Eur J Pharmacol* **393**:141-146.

Li P and Steinbach JH (2010) The neuronal nicotinic alpha4beta2 receptor has a high maximal probability of being open. *Br J Pharm* **160**:1906-1915.

Li SX, Huang S, Bren N, Noridomi K, Dellisanti CD, Sine SM and Chen L (2011) Ligand-binding domain of an alpha7-nicotinic receptor chimera and its complex with agonist. *Nat Neurosci* **14**:1253-1259.

Lucero LM, Weltzin MM, Eaton JB, Cooper JF, Lindstrom JM, Lukas RJ and Whiteaker P (2016) Differential alpha4(+)/(-)beta2 Agonist-binding Site Contributions to alpha4beta2 Nicotinic Acetylcholine Receptor Function within and between Isoforms. *J Biol Chem* **291**:2444-2459.

Mazurov A, Hauser T and Miller CH (2006) Selective alpha7 nicotinic acetylcholine receptor ligands. *Curr Med Chem* **13**:1567-1584.

Miller C (1989) Genetic manipulation of ion channels: a new approach to structure and mechanism. *Neuron* **2**:1195-1205.

Morales-Perez CL, Noviello CM and Hibbs RE (2016) X-ray structure of the human alpha4beta2 nicotinic receptor. *Nature* **538**:411-415.

Nelson ME, Kuryatov A, Choi CH, Zhou Y and Lindstrom J (2003) Alternate stoichiometries of alpha4beta2 nicotinic acetylcholine receptors. *Mol Pharmacol* **63**:332-341.

Nemecz A and Taylor P (2011) Creating an alpha7 nicotinic acetylcholine recognition domain from the acetylcholine-binding protein: crystallographic and ligand selectivity analyses. *J Biol Chem* **286**:42555-42565.

Newcombe J, Chatzidaki A, Sheppard TD, Topf M and Millar NS (2018) Diversity of Nicotinic Acetylcholine Receptor Positive Allosteric Modulators Revealed by Mutagenesis and a Revised Structural Model. *Mol Pharmacol* **93**:128-140.

Papke RL (2014) Merging old and new perspectives on nicotinic acetylcholine receptors. *Biochem Pharmacol* **89**:1-11.

Papke RL, Bagdas D, Kulkarni AR, Gould T, AlSharari S, Thakur GA and Damaj IM (2015) The analgesic-like properties of the alpha7 nAChR silent agonist NS6740

is associated with nonconducting conformations of the receptor. *NeuroPharm* **91**:34-42.

Papke RL, Boulter J, Patrick J and Heinemann S (1989) Single-channel currents of rat neuronal nicotinic acetylcholine receptors expressed in xenopus laevis oocytes. *Neuron* **3**:589-596.

Papke RL, Horenstein NA, Kulkarni AR, Stokes C, Corrie LW, Maeng CY and Thakur GA (2014) The activity of GAT107, an allosteric activator and positive modulator of alpha7 nicotinic acetylcholine receptors (nAChR), is regulated by aromatic amino acids that span the subunit interface. *J Biol Chem* **289**:4515-4531.

Papke RL, Kem WR, Soti F, López-Hernández GY and Horenstein NA (2009) Activation and desensitization of nicotinic alpha7-type acetylcholine receptors by benzylidene anabaseines and nicotine. *J Pharmacol Exp Ther* **329**:791-807.

Papke RL, Meyer EM and de Fiebre CM (1996) Differential discrimination between human and rat $_{a7}$ nAChR by GTS-21 and its primary metabolite, 4-OH,2 Methoxybenzylidene anabaseine., in *26th Annual Meeting of the Society for Neuroscience* p 602.604.

Papke RL and Papke JKP (2002) Comparative pharmacology of rat and human alpha7 nAChR conducted with net charge analysis. *Br J of Pharm* **137**:49-61.

Papke RL and Stokes C (2010) Working with OpusXpress: methods for high volume oocyte experiments. *Methods* **51**:121-133.

Papke RL, Stokes C, Muldoon P and Imad Damaj M (2013) Similar activity of mecamylamine stereoisomers in vitro and in vivo. *Eur J Pharmacol* **720**:264-275.

Papke RL, Stokes C, Williams DK, Wang J and Horenstein NA (2011) Cysteine accessibility analysis of the human alpha7 nicotinic acetylcholine receptor ligand-binding domain identifies L119 as a gatekeeper. *Neuropharmacology* **60**:159-171.

Papke RL and Thinschmidt JS (1998) The correction of alpha7 nicotinic acetylcholine receptor concentration-response relationships in *Xenopus* oocytes. *Neurosci Let* **256**:163-166.

Pavlov VA, Ochani M, Yang LH, Gallowitsch-Puerta M, Ochani K, Lin X, Levi J, Parrish WR, Rosas-Ballina M, Czura CJ, Larosa GJ, Miller EJ, Tracey KJ and Al-Abed Y (2007) Selective alpha7-nicotinic acetylcholine receptor agonist GTS-21 improves survival in murine endotoxemia and severe sepsis. *Crit Care Med* **35**:1139-1144.

Picciotto MR, Addy NA, Mineur YS and Brunzell DH (2008) It is not "either/or": activation and desensitization of nicotinic acetylcholine receptors both contribute to behaviors related to nicotine addiction and mood. *Prog Neurobiol* **84**:329-342.

Pieschl RL, Miller R, Jones KM, Post-Munson DJ, Chen P, Newberry K, Benitex Y, Molski T, Morgan D, McDonald IM, Macor JE, Olson RE, Asaka Y, Digavalli S, Easton A, Herrington J, Westphal RS, Lodge NJ, Zaczek R, Bristow LJ and Li YW (2017) Effects of BMS-902483, an alpha7 nicotinic acetylcholine receptor partial agonist, on cognition and sensory gating in relation to receptor occupancy in rodents. *Eur J Pharmacol* **807**:1-11.

Post-Munson DJ, Pieschl RL, Molski TF, Graef JD, Hendricson AW, Knox RJ, McDonald IM, Olson RE, Macor JE, Weed MR, Bristow LJ, Kiss L, Ahlijanian MK and Herrington J (2017) B-973, a novel piperazine positive allosteric modulator of the alpha7 nicotinic acetylcholine receptor. *Eur J Pharmacol* **799**:16-25.

Prickaerts J, van Goethem NP, Chesworth R, Shapiro G, Boess FG, Methfessel C, Reneerkens OA, Flood DG, Hilt D, Gawryl M, Bertrand S, Bertrand D and Konig G (2012) EVP-6124, a novel and selective alpha7 nicotinic acetylcholine receptor partial agonist, improves memory performance by potentiating the acetylcholine

response of alpha7 nicotinic acetylcholine receptors. *Neuropharmacology* **62**:1099-1110.

Quadri M, Garai S, Thakur GA, Stokes C, Gulsevin A, Horenstein NA and Papke RL (2019) Macroscopic and microscopic activation of alpha7 nicotinic acetylcholine receptors by the structurally unrelated ago-PAMs B-973B and GAT107. *Mol Pharmacol* **95**:43-61.

Rosas-Ballina M, Goldstein RS, Gallowitsch-Puerta M, Yang L, Valdes-Ferrer SI, Patel NB, Chavan S, Al-Abed Y, Yang H and Tracey KJ (2009) The selective alpha7 agonist GTS-21 attenuates cytokine production in human whole blood and human monocytes activated by ligands for TLR2, TLR3, TLR4, TLR9, and RAGE. *Mol Med* **15**:195-202.

Rosas-Ballina M and Tracey KJ (2009) Cholinergic control of inflammation. *J Intern Med* **265**:663-679.

Thakur GA, Kulkarni AR, Deschamps JR and Papke RL (2013) Expeditious Synthesis, Enantiomeric Resolution and Enantiomer Functional Characterization of (4-(4-bromophenyl)-3a,4,5,9b-tetrahydro-3H-cyclopenta[c]quinoline-8-sulfonamide (4BP-TQS) an Allosteric agonist –Positive Allosteric Modulator of alpha7 nAChR. *Journal of Medicinal Chemistry* **56**:8943-8947.

Uteshev VV, Meyer EM and Papke RL (2002) Activation and inhibition of native neuronal alpha-bungarotoxin-sensitive nicotinic ACh receptors. *Brain Res* **948**:33-46.

Verbitsky M, Rothlin CV, Katz E and Elgoyhen AB (2000) Mixed nicotinic-muscarinic properties of the alpha9 nicotinic cholinergic receptor. *Neuropharmacology* **39**:2515-2524.

Wada E, Wada K, Boulter J, Deneris E, Heinemann S, Patrick J and Swanson LW (1989) Distribution of alpha2, alpha3, alpha4, and beta2 neuronal nicotinic receptor

subunit mRNAs in the central nervous system: a hybridization histochemical study in the rat. *J Comp Neurol* **284**:314-335.

Wada K, Ballivet M, Boulter J, Connolly J, Wada E, Deneris E, Swanson L, Heinemann S and Patrick J (1988) Functional expression of a new pharmacological subtype of brain nicotinic acetylcholine receptor. *Science* **240**:330-334.

Wallace TL, Callahan PM, Tehim A, Bertrand D, Tombaugh G, Wang S, Xie W, Rowe WB, Ong V, Graham E, Terry AV, Jr., Rodefer JS, Herbert B, Murray M, Porter R, Santarelli L and Lowe DA (2011) RG3487, a novel nicotinic alpha7 receptor partial agonist, improves cognition and sensorimotor gating in rodents. *J Pharmacol Exp Ther* **336**:242-253.

Walsh RM, Jr., Roh SH, Gharpure A, Morales-Perez CL, Teng J and Hibbs RE (2018) Structural principles of distinct assemblies of the human alpha4beta2 nicotinic receptor. *Nature* **557**:261-265.

Wang H, Yu M, Ochani M, Amella CA, Tanovic M, Susarla S, Li JH, Yang H, Ulloa L, Al-Abed Y, Czura CJ and Tracey KJ (2003) Nicotinic acetylcholine receptor alpha7 subunit is an essential regulator of inflammation. *Nature* **421**:384-388.

Williams DK, Peng C, Kimbrell MR and Papke RL (2012) The Intrinsically Low Open Probability of alpha7 nAChR Can be Overcome by Positive Allosteric Modulation and Serum Factors Leading to the Generation of Excitotoxic Currents at Physiological Temperatures. *Mol Pharmacol* **82**:746-759.

Williams DK, Wang J and Papke RL (2011a) Investigation of the Molecular Mechanism of the Alpha7 nAChR Positive Allosteric Modulator PNU-120596 Provides Evidence for Two Distinct Desensitized States. *Mol Pharmacol* **80**:1013-1032.

Williams DK, Wang J and Papke RL (2011b) Positive allosteric modulators as an approach to nicotinic acetylcholine receptor-targeted therapeutics: Advantages and limitations. *Biochem Pharmacol* **82**:915-930.

Young GT, Zwart R, Walker AS, Sher E and Millar NS (2008) Potentiation of alpha7 nicotinic acetylcholine receptors via an allosteric transmembrane site. *Proc Natl Acad Sci U S A* **105**:14686-14691.

Zakrzewicz A, Richter K, Agne A, Wilker S, Siebers K, Fink B, Krasteva-Christ G, Althaus M, Padberg W, Hone AJ, McIntosh JM and Grau V (2017) Canonical and Novel Non-Canonical Cholinergic Agonists Inhibit ATP-Induced Release of Monocytic Interleukin-1beta via Different Combinations of Nicotinic Acetylcholine Receptor Subunits alpha7, alpha9 and alpha10. *Front Cell Neurosci* **11**:189.

Zhou Y, Nelson ME, Kuryatov A, Choi C, Cooper J and Lindstrom J (2003) Human alpha4beta2 acetylcholine receptors formed from linked subunits. *J Neurosci* **23**:9004-9015.

Footnotes

This research was supported by the National Institutes of Health Grants [R01-NS095899] and [R01-DA042072] to REH, and [R01-GM57481] to RLP, and [RO1-EY024717] to GAT.

Figure Legends

Figure 1. Amino acid sequences of nAChR subunits in the first and second transmembrane domains (TM1 and TM2, respectively) compared to the sequence of the 5HT3A receptor. The two residues shown to be most important in controlling the potentiating activity of PNU-120596 on α7 receptors (Young et al., 2008) are highlighted. Note that the aspartic acid (D) residue at 226 (α7 numbering) in TM1 is unique to 5HT3A. The sequences in TM2 are aligned so we can apply a local numbering system (Miller, 1989) for this subdomain. The 1' position, closest to the intracellular domain, is to the left and the 20' position is to the right. The other residue most critical for PNU-120596 potentiation was the 15' methionine (M254), which is unique to α7.

Figure 2. α4β2 double mutant data. Averaged raw data traces (± SEM) for α4β2 receptors with L15'M mutations in both subunits. Prior to averaging, the data from each cell were normalized to the peak amplitude of two initial 30 μM ACh control responses (see Methods). The average amplitude of the ACh controls was 325 ± 27 nA. The PNU-120596 data are the average of eight cells and the TQS data the average of four cells. The inset in the upper panels is an overlay of the ACh controls and the responses to ACh plus 10 μM PNU-120596.

Figure 3. α4β2 receptors with L15'M mutations in both subunits or single subunits. **A)** The average peak currents from cells recorded on the same day from different injection sets as indicated: α4β2, wild-type subunits; α4∗β2, $\alpha4^{L15'M}$ and wild-type β2 subunits; α4β2∗, wild-type α4 and $\beta2^{L15'M}$ subunits; α4*β2*, $\alpha4^{L15'M}$ and $\beta2^{L15'M}$ subunits. The data are the average peak currents for 5-8 oocytes. **B)** Data from the same cells in **A**, showing the responses to 30 μM ACh plus 10 μM TQS, normalized to the response to 30 μM ACh alone in the same cells. **C)** Data from panel B divided by the average ACh

control of the wild-type cells in panel **A**. **D)** Averaged raw data for the ACh and ACh plus TQS responses of cells expressing the L15'M mutation in either the α4 subunit (upper trace, n = 7) or the β2 subunit (lower trace, n = 4). **E**) Effects of TQS on desensitized receptors. After obtaining ACh control responses, 30 μM nicotine was applied to cells expressing α4β2L15'M receptors. This concentration of nicotine results in reduction (desensitization) of approximately 55% of the control ACh response (not shown). Under these conditions, the application of 1 μM TQS alone produced a large and protracted response (n = 8). The average responses, normalized to the initial ACh controls, are represented by the black line, and the shaded area shows the SEM at each point. Each segment represents 210 s of recording. The amplitude scale bar is based on the average peak currents of the initial ACh control responses.

Figure 4. ACh and TQS responses of $\alpha4\beta2_{L15'M}$ receptors. **A)** The ACh concentration-response relationship of cells expressing wild-type α4 and $\beta2_{L15'M}$ subunits (n = 7). ACh was applied at progressively higher concentrations in alternation with repeated control applications of 30 μM ACh to ensure that there was no rundown or cumulative desensitization through the course of the experiment. Data were normalized to the ACh maximum response. As noted in the text, the data could be fit by either a one-site or two-site model. The curve fit shown is for the one-site model that indicated an EC_{50} = 5.0 ± 0.6 μM. **B)** The concentration-response relationship for TQS potentiation of ACh responses of cells expressing wild-type α4 and $\beta2_{L15'M}$ subunits; the data are the average peak current responses from 4 to 7 cells at the varying concentrations, normalized to their respective ACh controls. Cells could only be exposed to single TQS applications, and at the highest concentration several cells failed voltage clamp. **C**) Averaged raw data traces for TQS-potentiated responses up to 10 μM shown in panel **B**, illustrating the protracted activation following single co-applications of ACh and TQS. Note that when ACh was

JPET Fast Forward. Published on June 7, 2019 as DOI: 10.1124/jpet.119.259499
This article has not been copyedited and formatted. The final version may differ from this version.

applied again after the co-application of 30 μM ACh and 30 μM TQS, all cells failed voltage clamp (not shown).

Figure 5. Responses of α4β2$_{L15'M}$ receptors to the ago-PAM GAT107 and its inactive isomer. **A)** The co-application 10 μM GAT107 with 30 μM ACh produced a significant potentiation ($p < 0.01$ $n = 8$). **B)** The application 10 μM GAT107 alone did not produce allosteric activation of α4β2∗ receptors. However, when ACh was applied following the application of GAT107 alone, there was a significant residual potentiation ($p < 0.01$ $n = 7$), as shown in the inset. **C)** GAT106, the 4BP-TQS isomer that is inactive on α7 (Thakur et al., 2013), did not produce any potentiation of α4β2$_{L15'M}$ receptor ACh-evoked responses. **D)** Activity of TQS isomers. Cells were injected with α4 and β2L15'M or wild-type α7. After two control applications of ACh (30 μM for α4β2L15'M or 60 μM for α7), ACh was co-applied with 300 nM of either the (+) or (-) isomer of TQS. Responses were normalized to the average of the ACh controls for each cell. (+)-TQS produced no significant potentiation compared to ACh alone, while (-)-TQS significantly ($p < 0.001$) potentiated responses of both receptor types. The addition of 3 μM (+)-TQS decreased responses compared to responses obtained with 300 nM (-)-TQS alone ($p < 0.01$, $n = 7$ for α4β2L15'M, and $p < 0.05$, $n = 8$ for α7). α4β2L15'M responses were measured as peak currents; α7 responses were measured as net charge. **E)** The X-ray crystal structure determined for (-)-TQS (see Methods). **F)** The structure is for (-)-TQS displaying the absolute stereochemistry, followed by an overlay structure for TQS and GAT107 (red color highlights the fused benzene ring found in TQS, not in GAT107), and far right, the structure of GAT107 showing absolute stereochemistry.

Figure 6. Activation and potentiation of α4β2$_{L15'M}$ receptors by the novel TQS analog GAT927. **A)** The averaged normalized raw data ($n = 5$) for cells expressing α4β2$_{L15'M}$ receptors to the application of 10 μM GAT927 (structure shown in insert). Note the

strong potentiation of subsequent ACh applications following the application of GAT927. **B)** Responses of α4β2$_{L15'M}$ receptors to GAT927 applied alone. The data are averaged peak currents (± SEM, n = 4-7), normalized to 30 μM ACh control responses from the same cells. Note that following the application of concentrations of GAT927 ≥ 30 μM applied alone, subsequent applications of ACh produced responses too large to be voltage clamped. These data were unsuitable to be fit to the Hill equation since there was no detectable plateau in the response. **C)** Responses of α4β2$_{L15'M}$ receptors to GAT927 co-applied with 30 μM ACh. The data are averaged peak currents (± SEM, n = 4-7), normalized to 30 μM ACh control responses from the same cells. Note that following the co-application of concentrations of GAT927 > 10 μM, responses were too large to be voltage clamped. These data were unsuitable to be fit to the Hill equation since there was no detectable plateau in the response.

Figure 7. Effects of GAT927 on HSα4β2 receptors with different numbers of mutant β subunits. **A)** The configuration of receptors formed with β2−6−α4 concatamer (Zhou et al., 2003) with or without the β2L15'M mutation. All receptors had the α4:β2 stoichiometry of 2:3, with 0, 1, 2, or 3 mutant beta subunits as indicated. All cells were injected on the same day and recorded the same number of days (7) following injection. **B)** The average amplitude of the ACh control responses (± SEM, n = 5-7). ACh responses of receptors containing 2 or 3 mutant subunits were significantly lower than wild-type receptors ($p < 0.001$ n = 5-6). **C)** The potentiation of 30 μM ACh responses normalized to the control ACh responses in the same cells. **D)** The average (± SEM) amplitude in μA of the responses to 30 μM ACh co-applied with 3 μM GAT927 (n = 5-7). While the potentiated responses of all receptors containing any number of mutant β subunits were greater than wild-type receptors ($p < 0.001$), there were no significant differences among the receptors containing any number of mutant subunits. **E)** Average peak current responses in μA of cells through the progress of an experiment where there

were first two control ACh applications followed by a co-application of 30 μM ACh plus 3 μM GAT 927, then two subsequent ACh applications. **F)** Average peak current responses in μA of cells through the progress of an experiment where there were first two control ACh applications followed by an application of 10 μM GAT 927 alone, then two subsequent ACh applications.

Figure 8. Effects of mutant number and position. Wild-type α7 and α7M254L were co-expressed alone or at various ratios so that the total RNA injected was held constant. Plotted are the average peak currents to two initial ACh controls (left axis) and the averaged normalized net charge responses potentiated by the co-application of 1 μM (racemic) TQS (right axis). There were no significant differences among the ACh responses (one-way ANOVA). When the percentage of wild-type RNA was less than 50%, the potentiation was less ($p < 0.05$) than with 100% α7 wild-type.

Figure 9. Evaluation of HS and LS α4β2 analogs with β2L15'M in the binding sites and wild-type α4 or β2 in the accessory subunit position. **A)** The average responses to 100 μM ACh. Responses of receptors with a β2 subunit in the accessory position were smaller than those with an α4 subunit ($P < 0.05$). **B)** Responses to 100 μM ACh relative to 10 μM ACh in the same cells. Responses of receptors with an α4 subunit in the accessory position to 100 μM ACh were significantly larger than their responses to 10 μM ACh ($p < 0.01$), while those with an accessory β2 subunit were not increased. **C)** The normalized responses to 100 μM ACh ± 10 μM TQS. Responses of receptors with a β2 subunit in the accessory position were significantly larger than those with an α4 subunit in the accessory position ($p > 0.05$). **D)** Potentiated responses to 100 μM ACh plus 10 μM TQS in μA. In terms of absolute magnitude, responses of receptors with a β2 subunit in the accessory position were significantly smaller than those with an α4 subunit in the accessory position ($p > 0.05$).

Figure 10. Comparison of the potentiation of α4β2$_{L15'M}$ receptors and α7 by TQS and GAT927 and other published PAMs. Data are the averaged responses to ACh (30 μM for α4β2$_{L15'M}$ receptors and 60 μM for α7) co-applied with the indicated PAM at 10 μM, relative to the responses to ACh alone.

Figure 11. The co-expression of β2$_{L15'M}$ with the alternative α subunits, α2 or α3. Shown are the averaged raw data responses of 4-6 cells, normalized to 100 μM ACh control responses in the same cell.

Figure 12. The co-expression of β4$_{L15'M}$ with alternative α subunits. Shown are the averaged raw data responses of 4-6 cells, normalized to 100 μM ACh control responses in the same cells. TQS was co-applied at a concentration of 10 μM.

Figure 13. Location and differential effects of residues affecting PAM activity in α4β2 and α7. **A)** Left, a β2-α4 interface from the heteropentameric α4β2 receptor (PDB: 6CNJ) is shown. β2 is in blue, and α4 is in green. The 15' residue of M2 implicated in binding to TQS and PNU-120596 is shown as red spheres, while A227, associated with the potentiating effects of PNU, is shown in orange spheres. Right, the active (-) isomer and inactive (+) isomers of TQS are shown with magenta spheres, and PNU-120596 (PNU) is shown with bronze spheres; these are shown to scale with the TM regions in the center. **B)** The differential effects of the M254L and A226D mutations in α7 on potentiation by PNU-120596 and TQS.

JPET Fast Forward. Published on June 7, 2019 as DOI: 10.1124/jpet.119.259499
This article has not been copyedited and formatted. The final version may differ from this version.

Table 1. effects of L15'M mutation (*) in muscle-type nAChR

Peak current responses in μA

Subunits	30 μM ACh	ACh + 10 μM TQS	N
α1β1εδ	0.31 ± 0.19	0.17 ± 0.12	7
α1∗β1εδ	0.028 ± 0.005	0.013 ± 0.002†††	8
α1β1ε∗δ	1.05 ± 0.34	0.36 ± 0.12†	8
α1β1γ∗δ	8.70 ± 1.88*	6.68 ± 2.09††	8
α1β1εδ∗	1.34 ± 0.41*	0.68 ± 0.23†	7
α1β1ε∗δ∗	8.79 ± 1.92*	5.8 ± 1.5†††	8
α1β1∗εδ	NA	NA	

ACh controls compared to wildtype, unpaired t-tests, * $p < 0.05$

ACh plus TQS compared to ACh alone, paired t-tests, † $p < 0.05$, †† $p < 0.01$, ††† $p < 0.001$

JPET Fast Forward. Published on June 7, 2019 as DOI: 10.1124/jpet.119.259499
This article has not been copyedited and formatted. The final version may differ from this version.

Figure 1

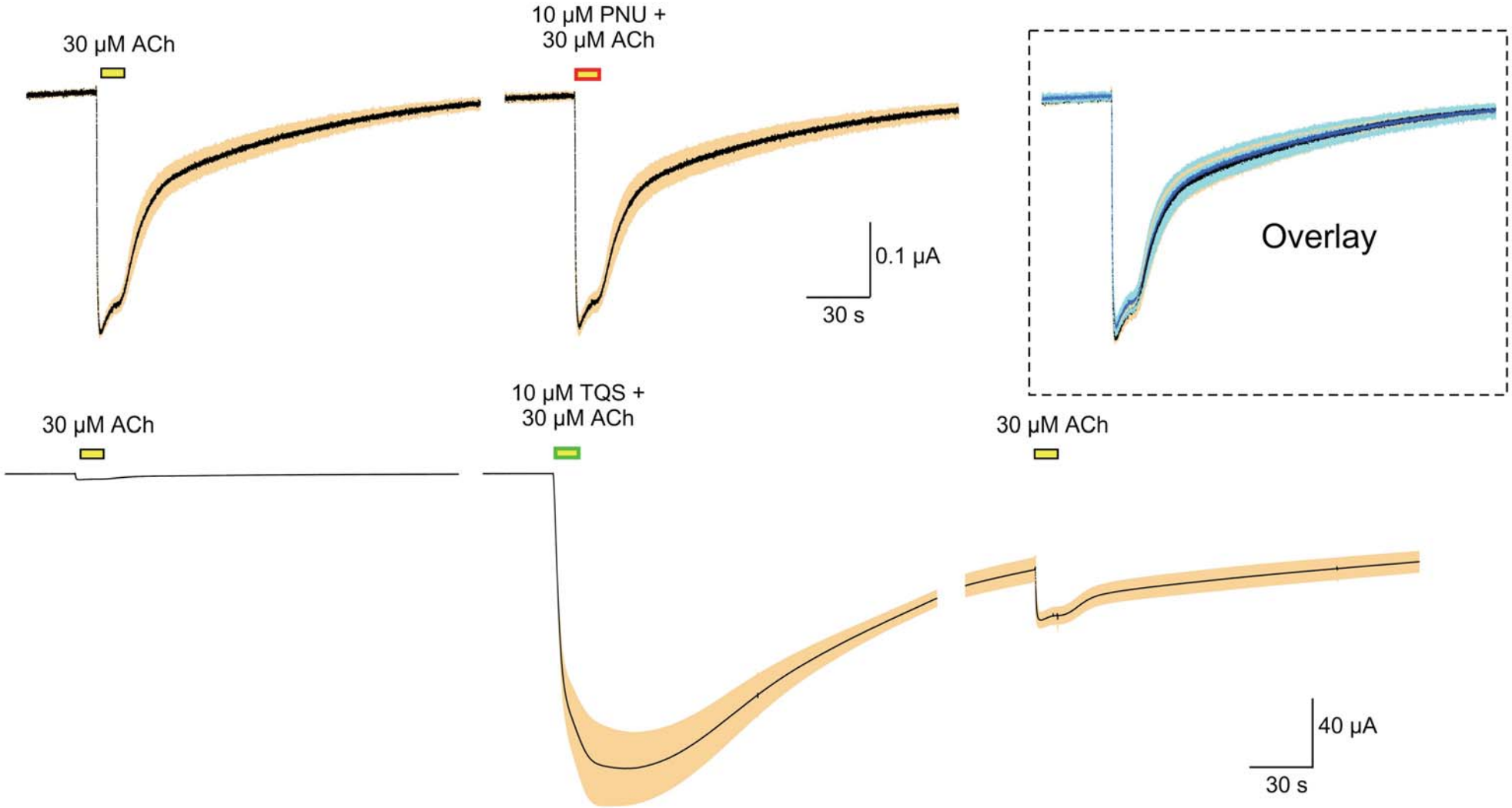

Figure 2

JPET Fast Forward. Published on June 7, 2019 as DOI: 10.1124/jpet.119.259499
This article has not been copyedited and formatted. The final version may differ from this version.

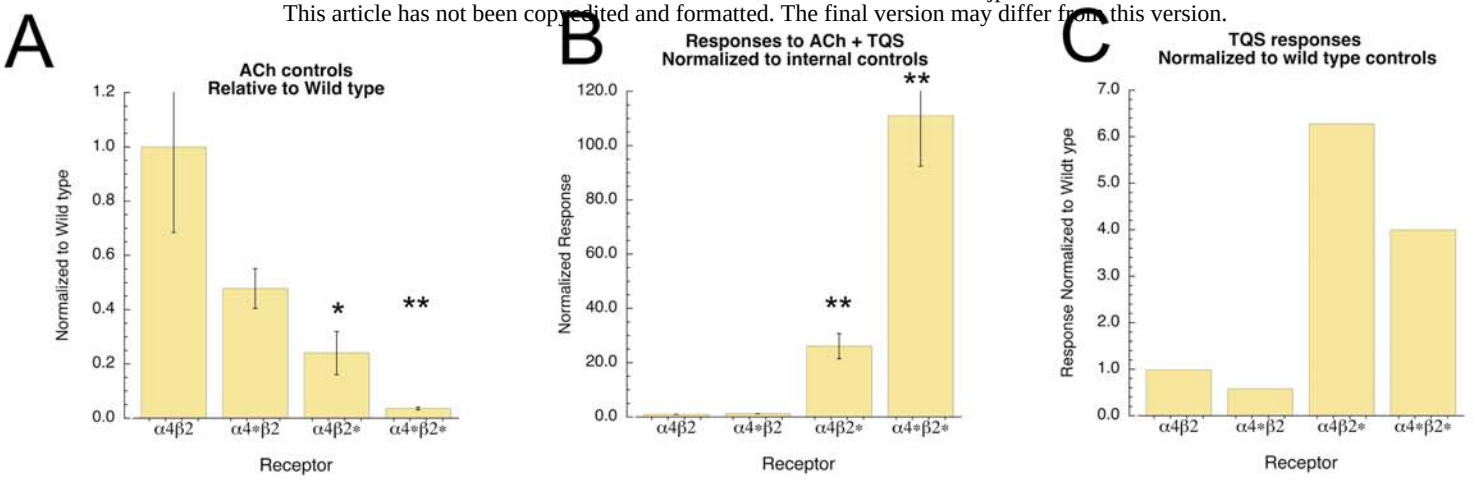

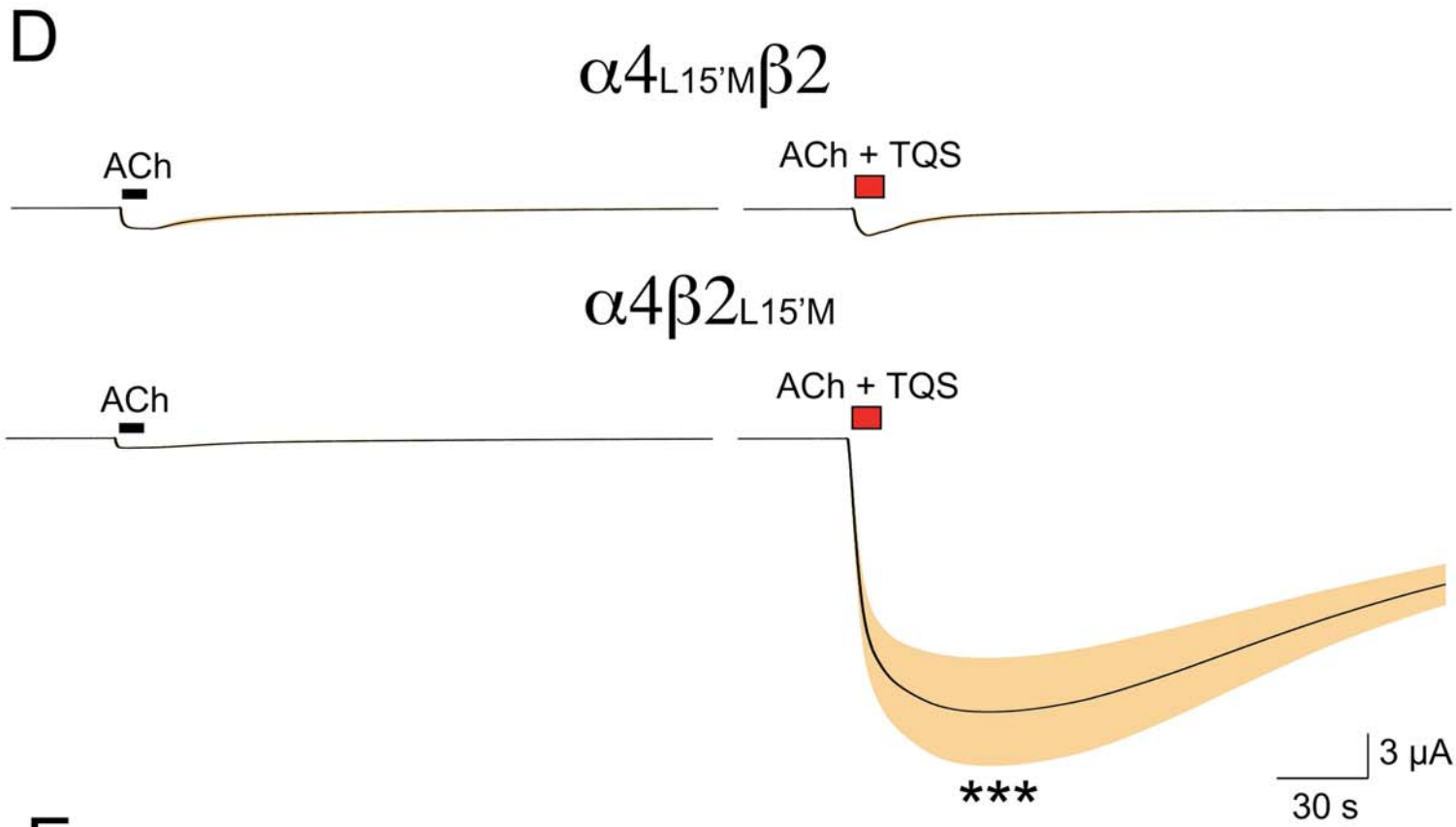

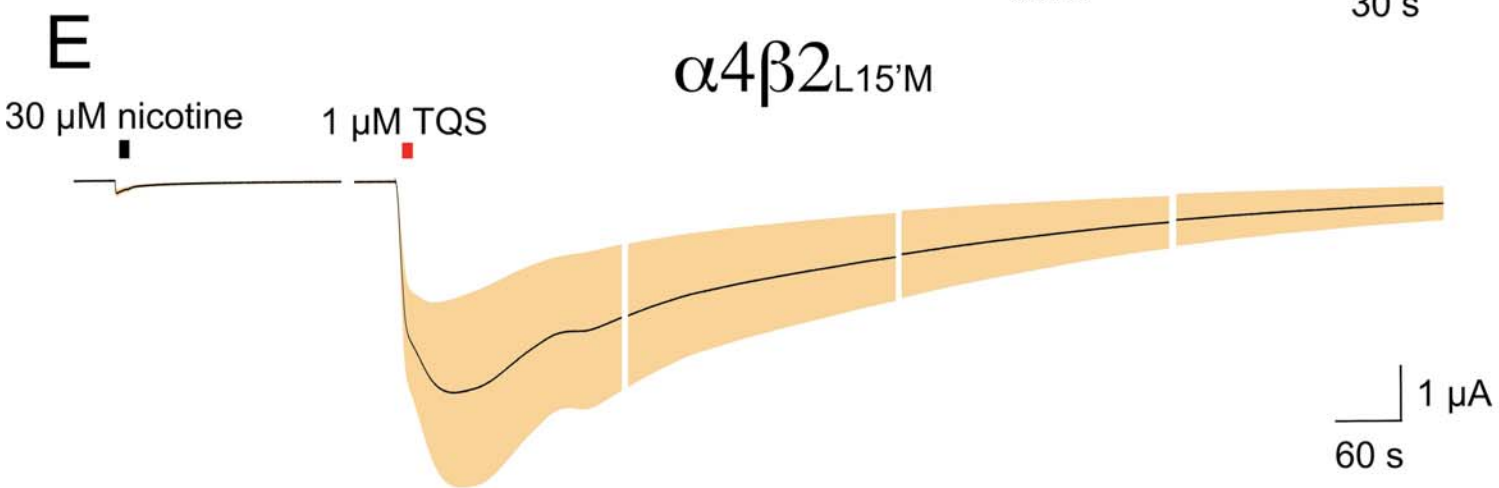

Figure 3

JPET Fast Forward. Published on June 7, 2019 as DOI: 10.1124/jpet.119.259499
This article has not been copyedited and formatted. The final version may differ from this version.

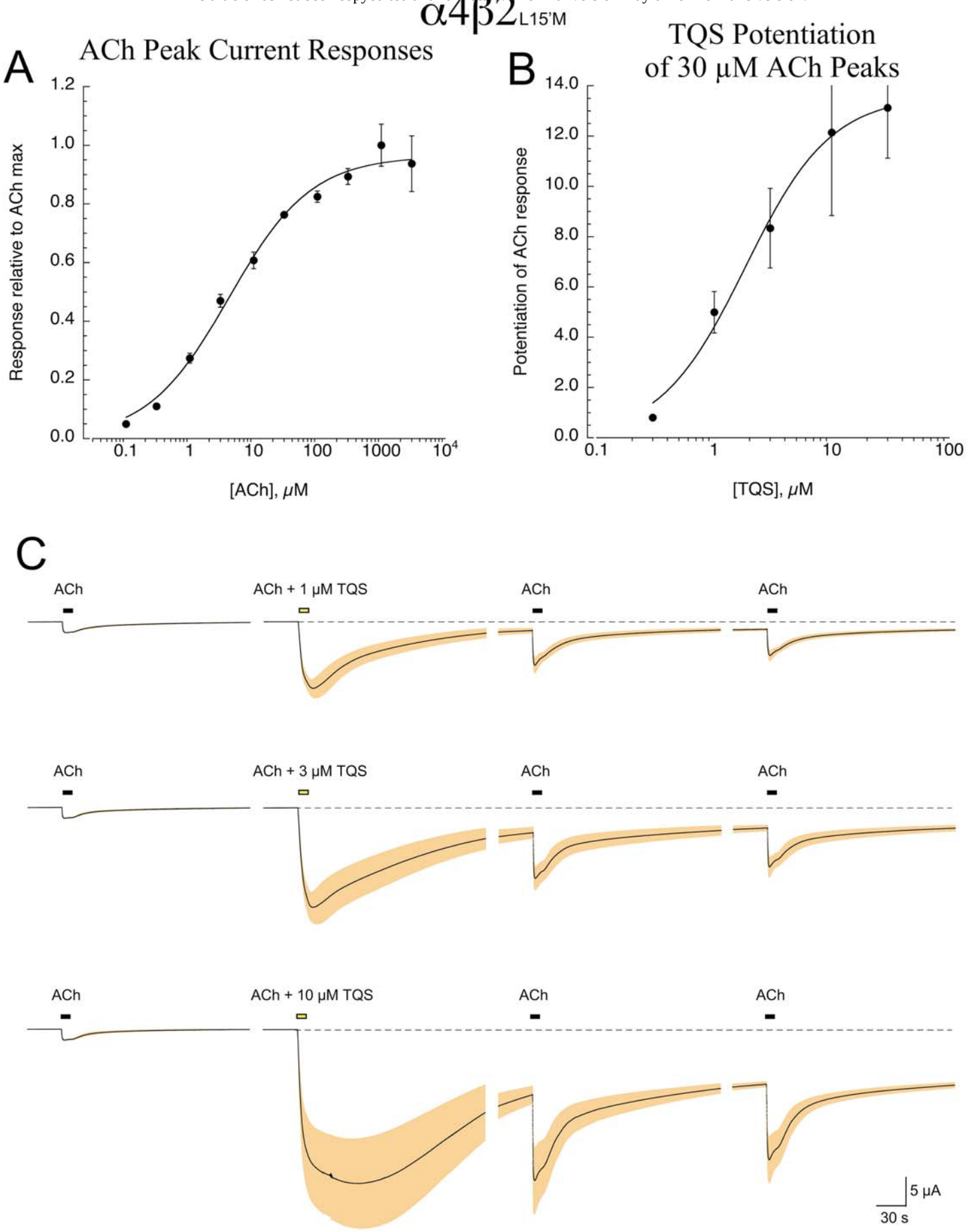

Figure 4

JPET Fast Forward. Published on June 7, 2019 as DOI: 10.1124/jpet.119.259499
This article has not been copyedited and formatted. The final version may differ from this version.

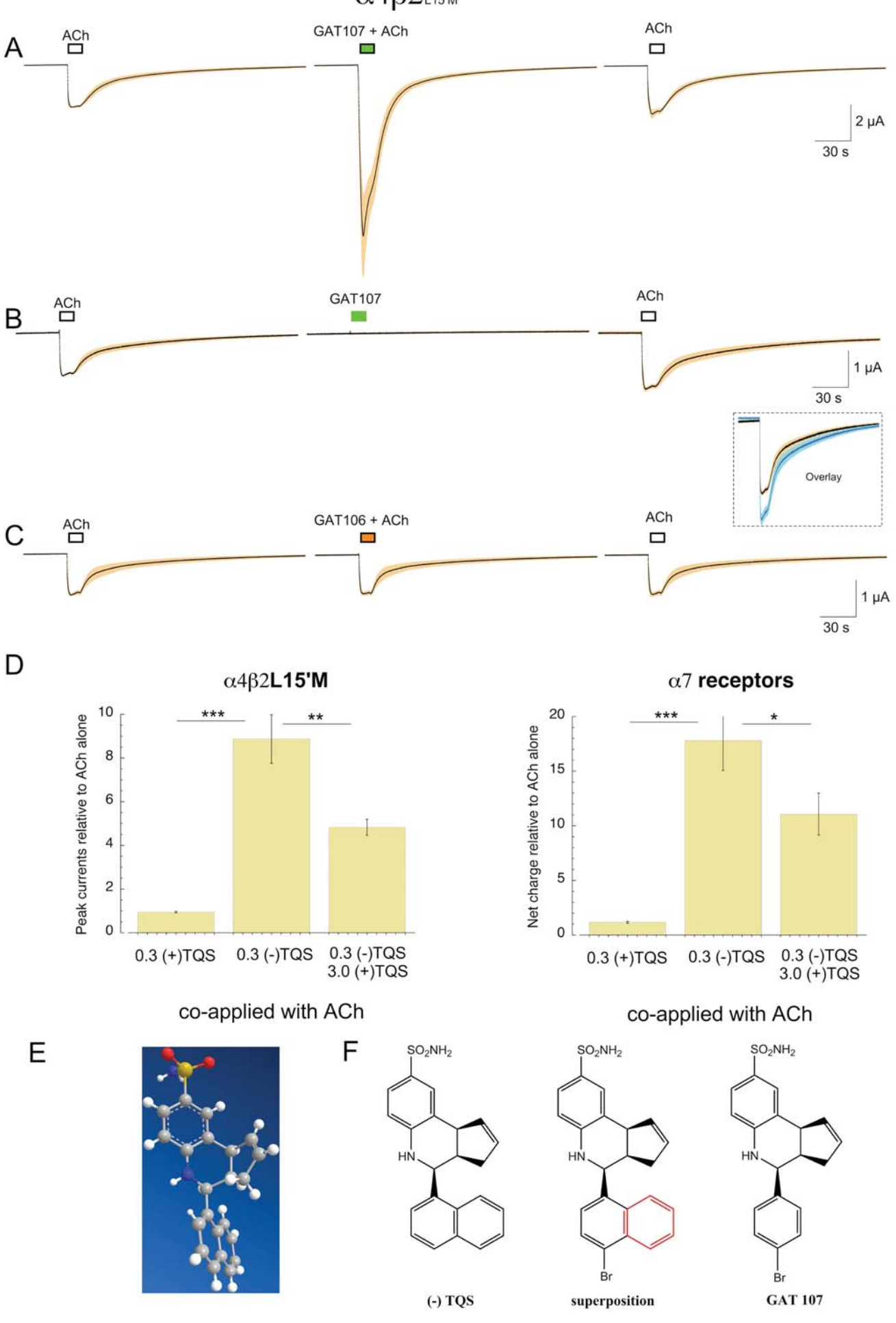

Figure 5

JPET Fast Forward. Published on June 7, 2019 as DOI: 10.1124/jpet.119.259499
This article has not been copyedited and formatted. The final version may differ from this version.

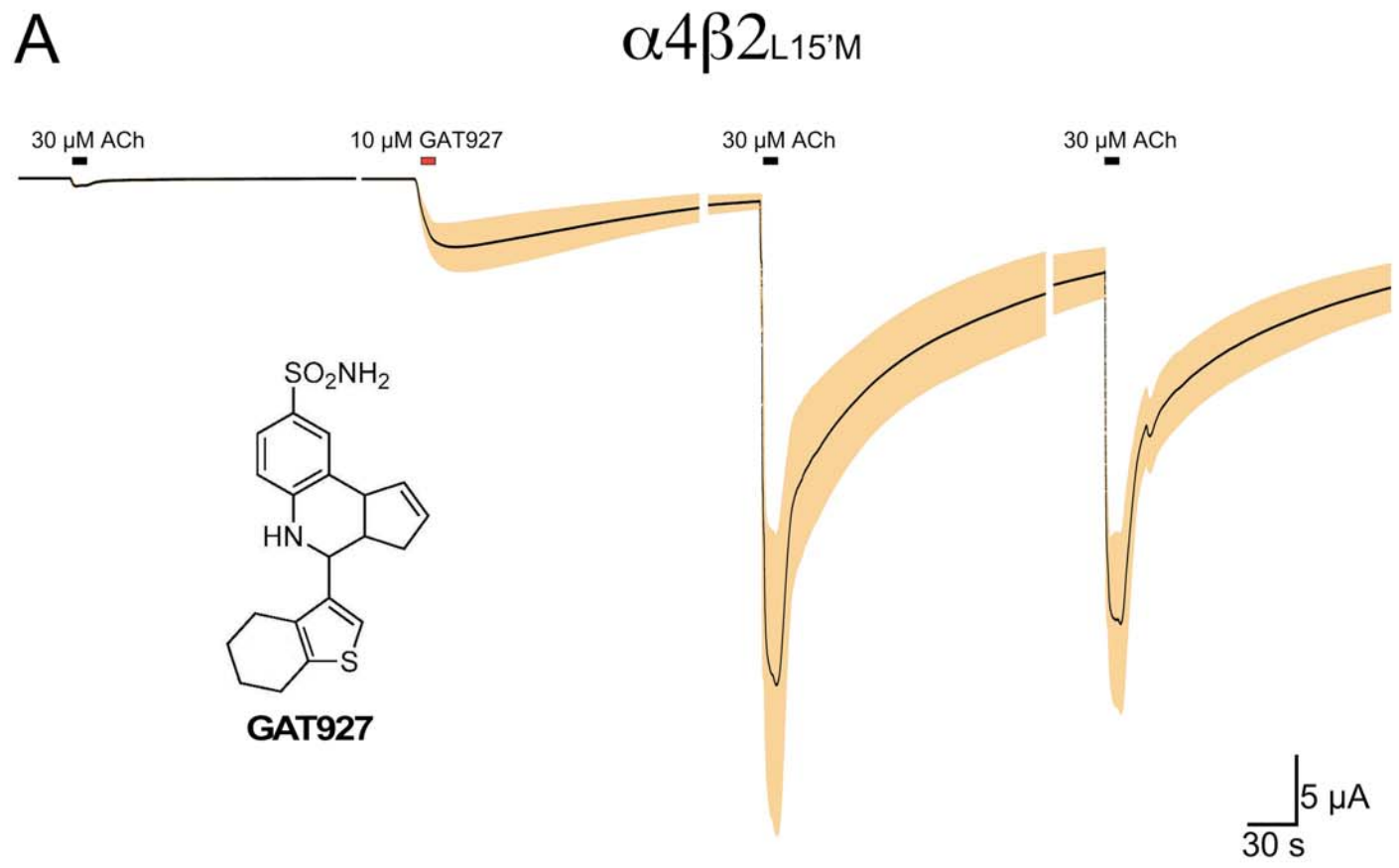

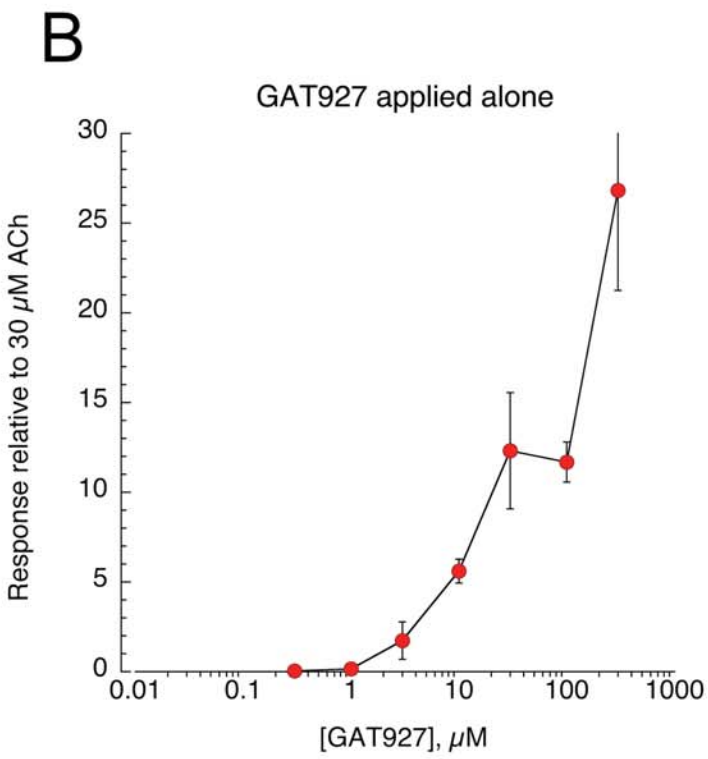

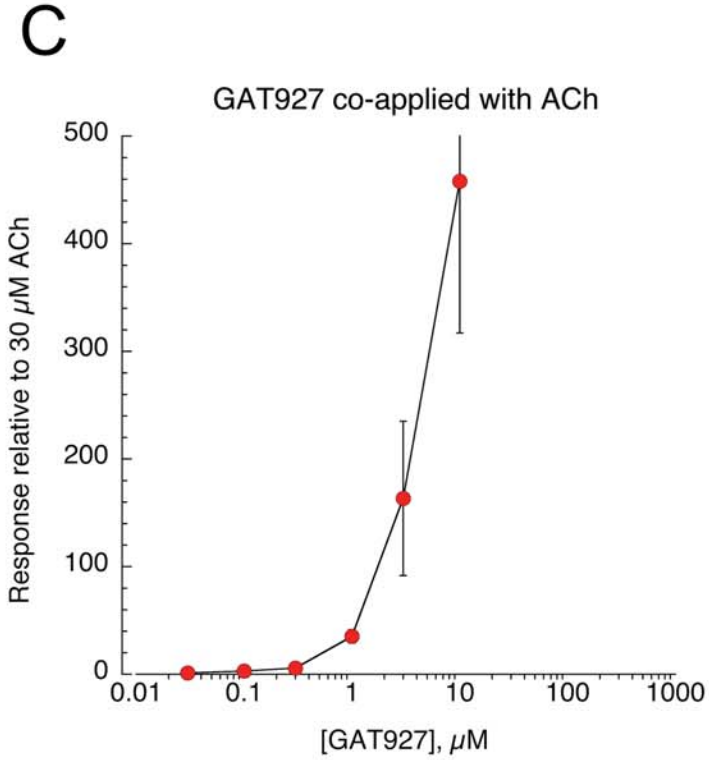

Figure 6

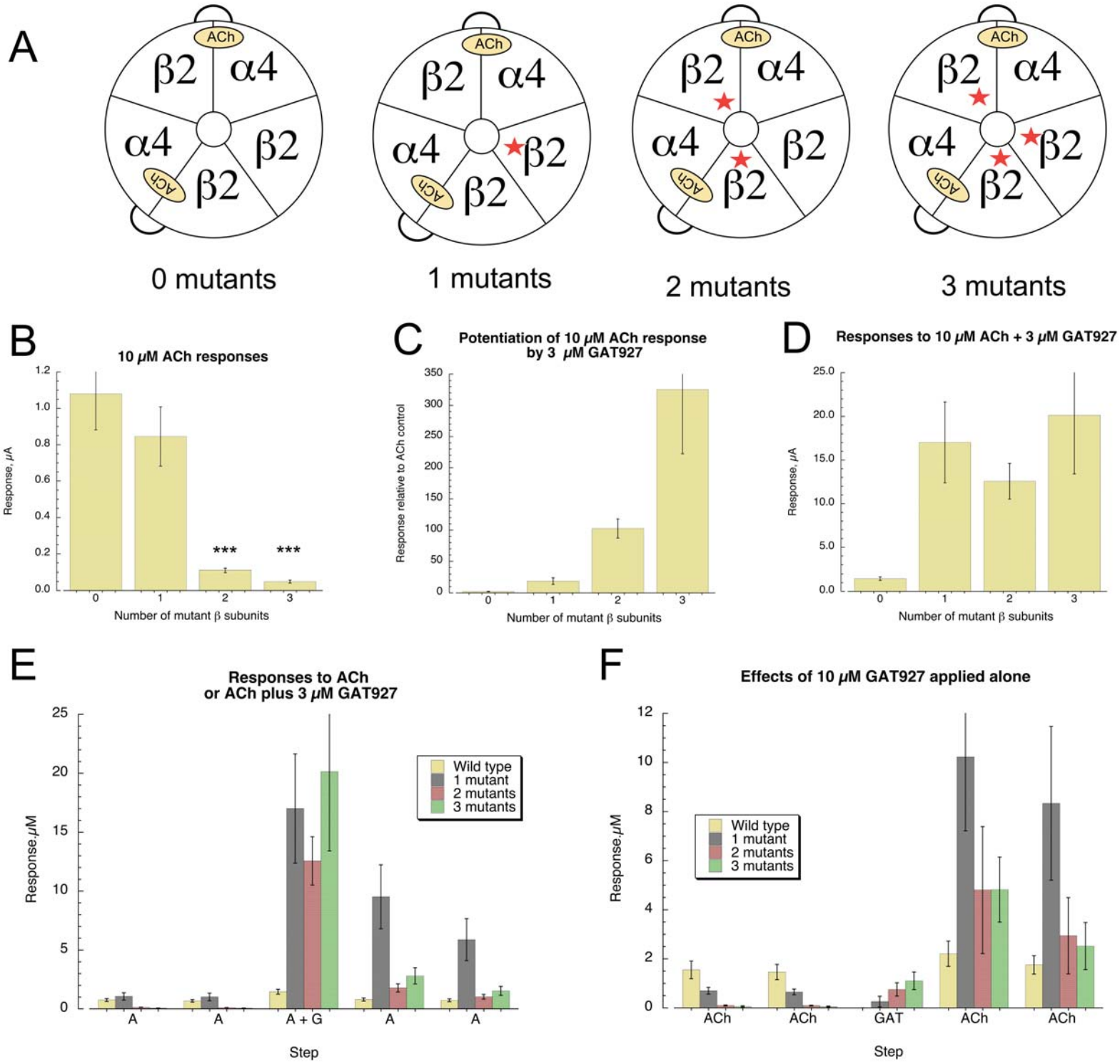

Figure 7

JPET Fast Forward. Published on June 7, 2019 as DOI: 10.1124/jpet.119.259499
This article has not been copyedited and formatted. The final version may differ from this version.

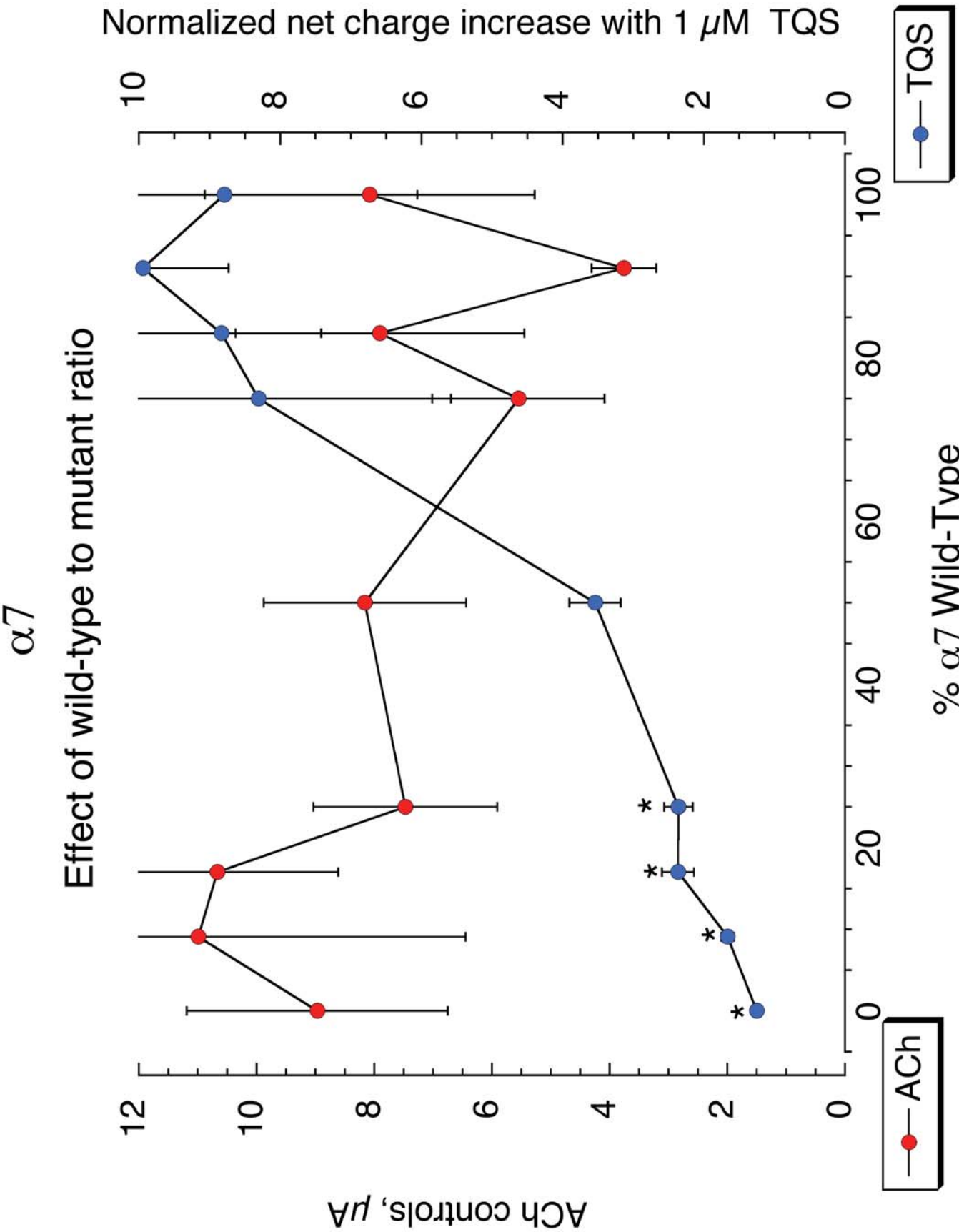

Figure 8

JPET Fast Forward. Published on June 7, 2019 as DOI: 10.1124/jpet.119.259499
This article has not been copyedited and formatted. The final version may differ from this version.

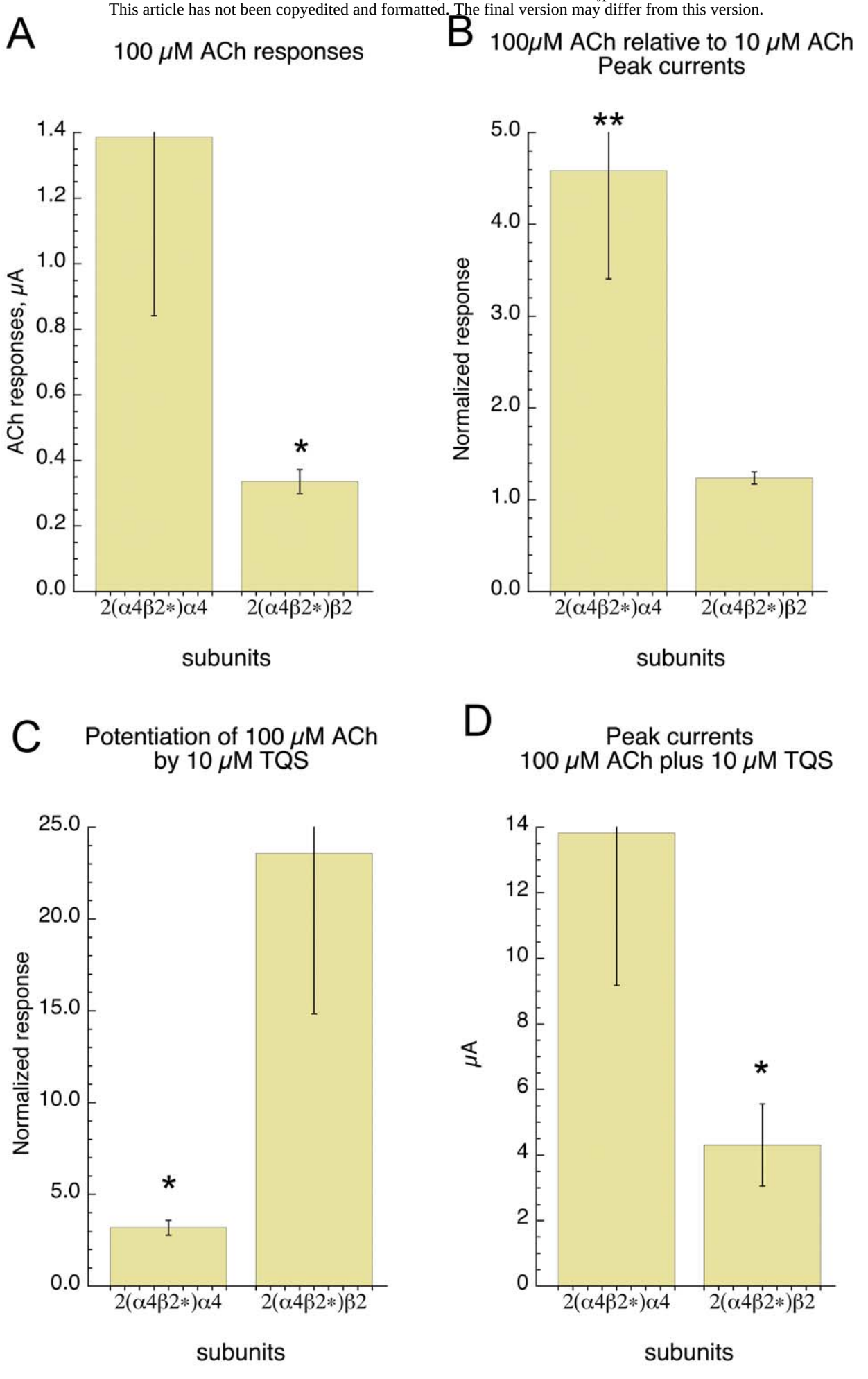

Figure 9

JPET Fast Forward. Published on June 7, 2019 as DOI: 10.1124/jpet.119.259499
This article has not been copyedited and formatted. The final version may differ from this version.

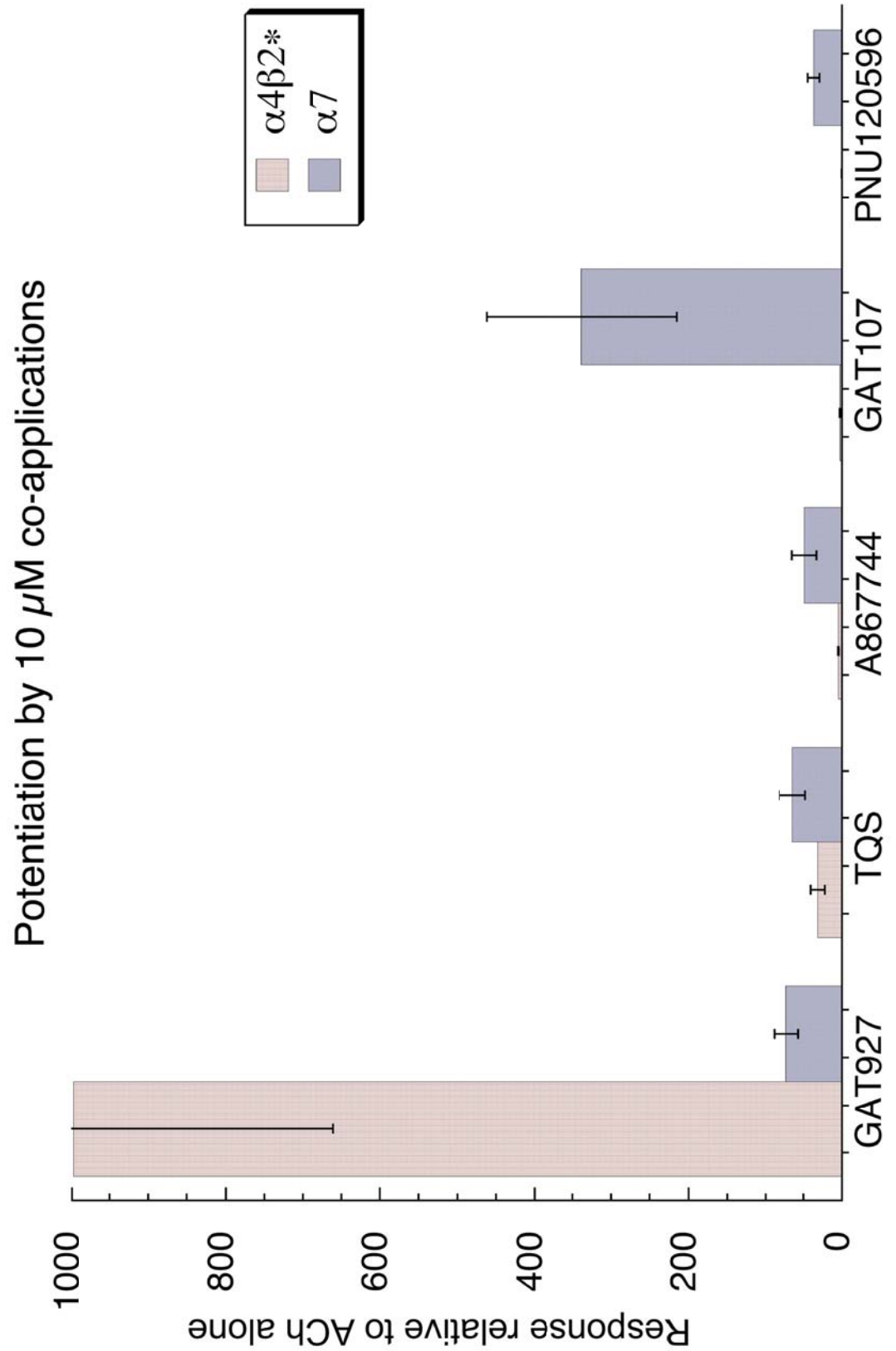

Figure 10

JPET Fast Forward. Published on June 7, 2019 as DOI: 10.1124/jpet.119.259499
This article has not been copyedited and formatted. The final version may differ from this version.

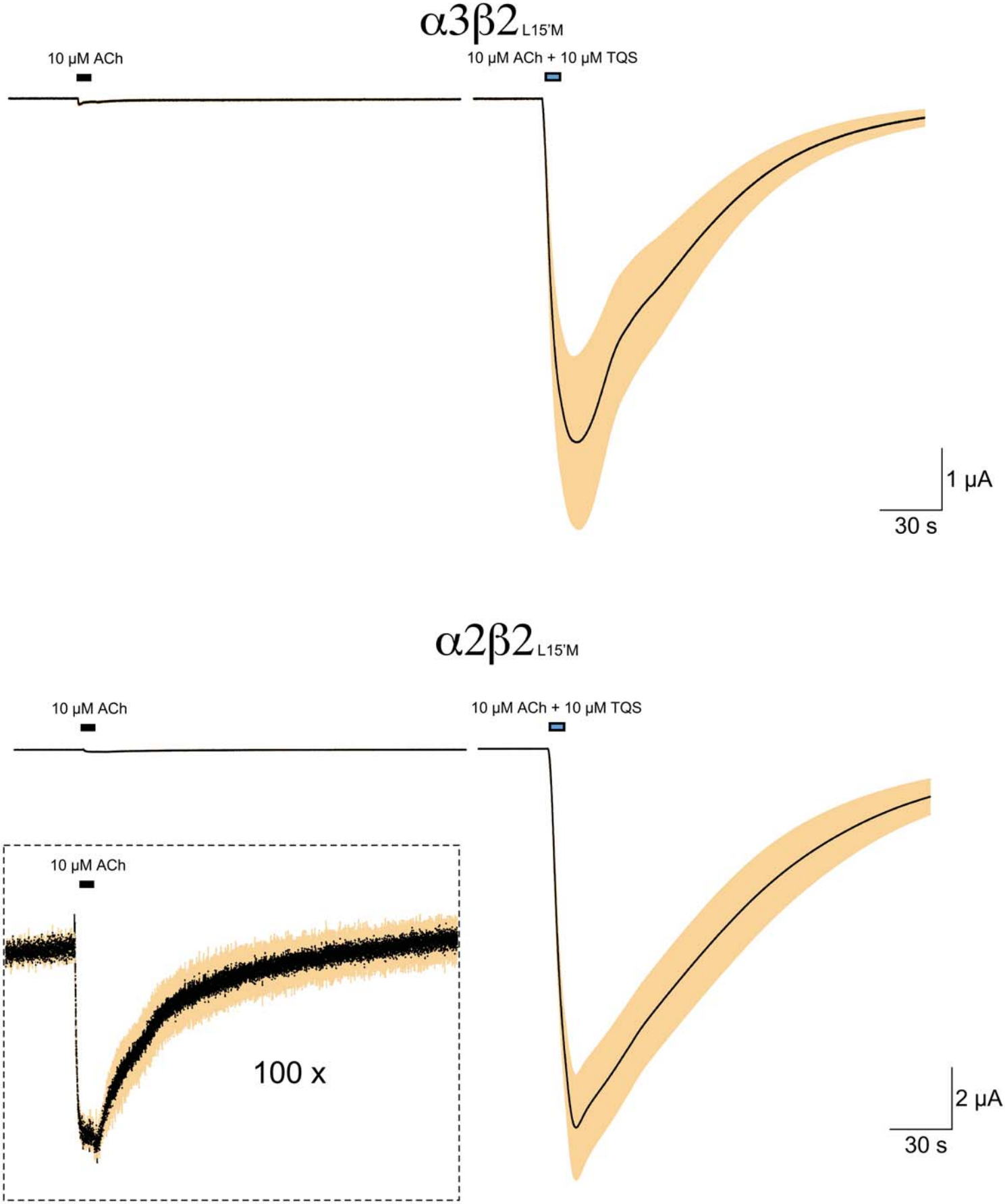

Figure 11

JPET Fast Forward. Published on June 7, 2019 as DOI: 10.1124/jpet.119.259499
This article has not been copyedited and formatted. The final version may differ from this version.

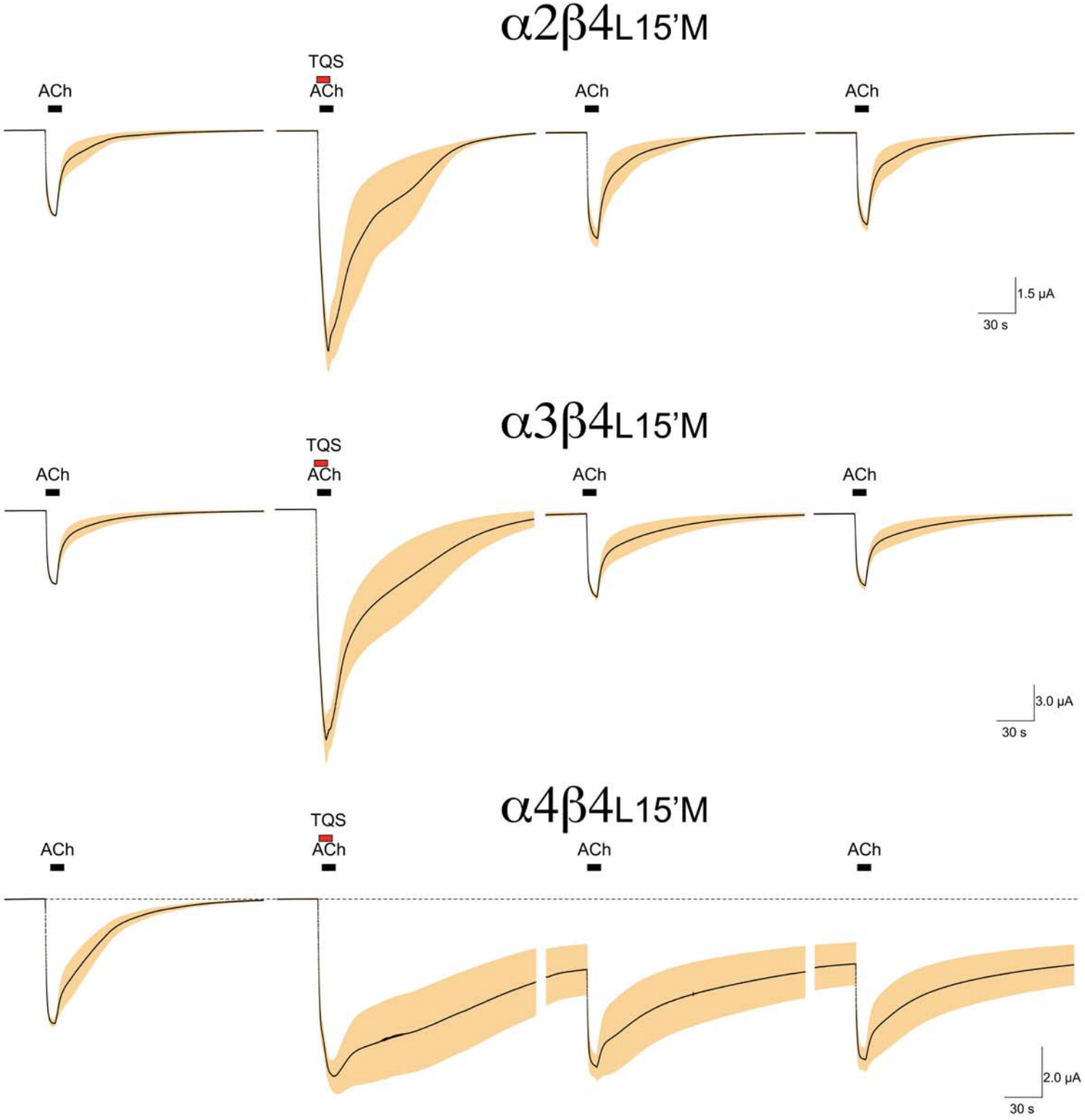

Figure 12

JPET Fast Forward. Published on June 7, 2019 as DOI: 10.1124/jpet.119.259499
This article has not been copyedited and formatted. The final version may differ from this version.

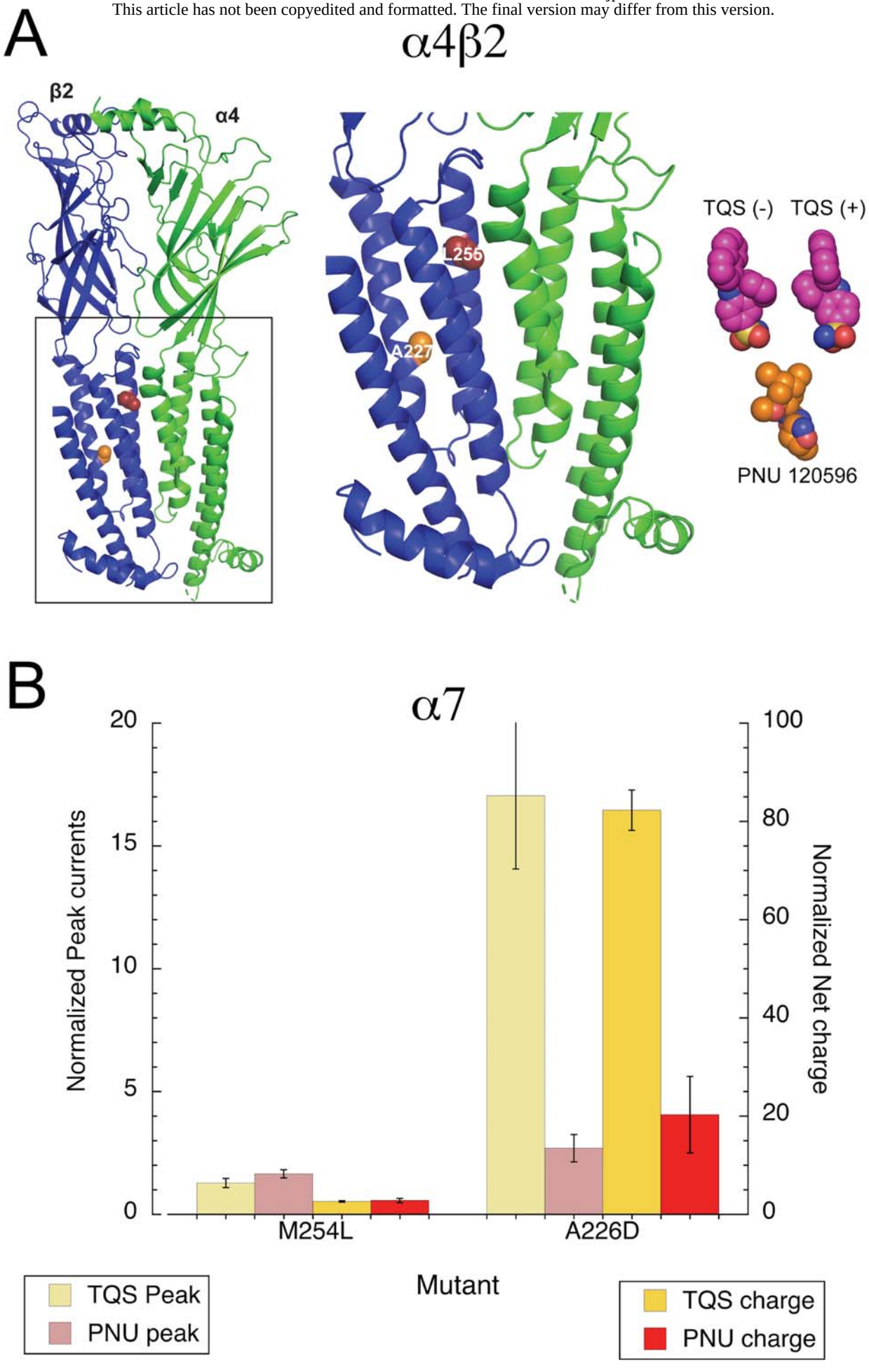

Figure 13